IOWA STATE UNIVERSITY
Digital Repository

Retrospective Theses and Dissertations

Iowa State University Capstones, Theses and Dissertations

1988

Automated angular scans to determine flaw orientation for use in model-based flaw reconstruction

James A. Crowder
Iowa State University

Follow this and additional works at: https://lib.dr.iastate.edu/rtd

 Part of the Electrical and Computer Engineering Commons

Recommended Citation
Crowder, James A., "Automated angular scans to determine flaw orientation for use in model-based flaw reconstruction" (1988). *Retrospective Theses and Dissertations*. 228.
https://lib.dr.iastate.edu/rtd/228

This Thesis is brought to you for free and open access by the Iowa State University Capstones, Theses and Dissertations at Iowa State University Digital Repository. It has been accepted for inclusion in Retrospective Theses and Dissertations by an authorized administrator of Iowa State University Digital Repository. For more information, please contact digirep@iastate.edu.

www.manaraa.com

Automated angular scans to determine flaw orientation for use in model-based flaw reconstruction

by

James Albert Crowder

A Thesis Submitted to the

Graduate Faculty in Partial Fulfillment of the

Requirements for the Degree of

MASTER OF SCIENCE

Department: Electrical Engineering and Computer Engineering

Major: Electrical Engineering

Approved:

Steve H. Russell
In Charge of Major Work

For the Major Department

For the Graduate College

Iowa State University
Ames, Iowa

1988

TABLE OF CONTENTS

LIST OF FIGURES

LIST OF TABLES

I. INTRODUCTION

A. Background

In manufacturing, the ability to detect and characterize failure-initiating flaws is important in the assurance of the structural integrity of materials and components. One major technique in the detection and characterization of such flaws is ultrasonics. In recent years, significant advances have been made in inverse ultrasonic scattering in the region where the ultrasonic wavelength is of the same order as the "radius"[1] of the flaw [1, 2, 3, 4]. Such work is based on physical models that describe the interaction between an elastic wave and the flaw for both long and intermediate wavelength inverse scattering [5, 6].

To exploit these theoretical advances in elastic wave inverse scattering, an automated multiviewing ultrasonic transducer system [7, 8] and associated software has been designed and built in order to perform characterization and analysis of volumetric flaws[2] [8, 9]. The flaw is characterized by its size, shape, and orientation within a material. Utilizing inverse ultrasonic scattering theories [7, 10], signal processing algorithms perform three-dimensional reconstruction by finding an ellipsoid that best fits the inverse scattering data

---

[1]The term radius is a loose term here that refers to an indication of size.

[2]Volumetric as opposed to crack-like flaws.

taken from many independent perspectives within a specified aperture.

The automated multiviewing system consists of six ultrasonic transducers equally spaced at 60° intervals about the device center. Figure 1 shows the six transducers positioned above a sample. Each transducer can be moved radially toward the center, with two of the transducers having the capability of moving completely into the center. Each transducer may be tilted toward the central axis, and may be moved along its own respective acoustic axis to allow for equalization of the acoustic wave propagation time. The flaw

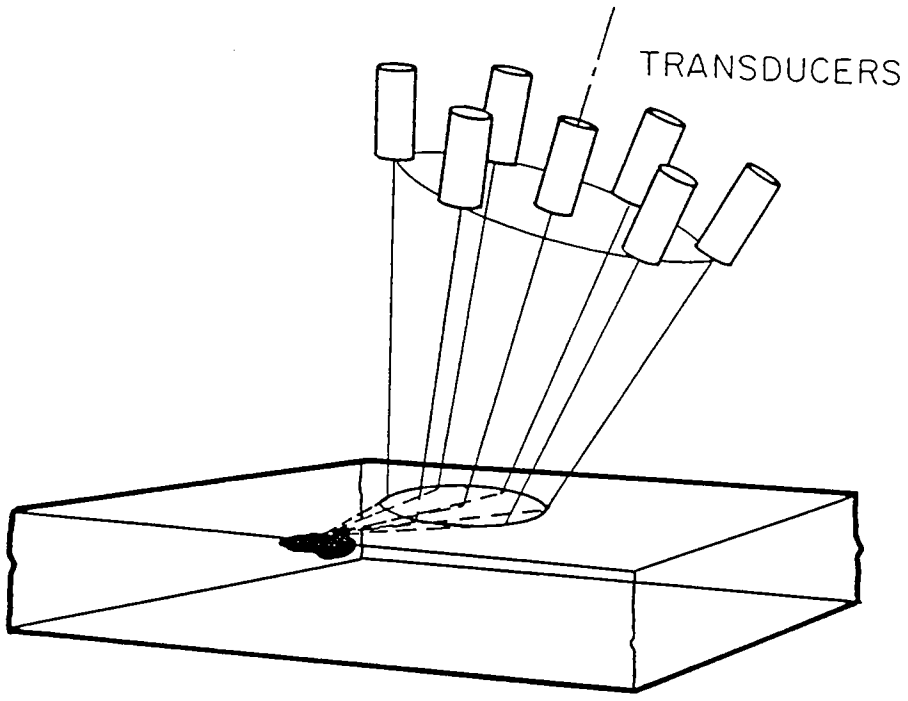

Figure 1. Multiviewing Transducers

reconstruction algorithm makes use of thirteen backscatter waveforms (see Appendix A) acquired in a conical pattern where the center of the pattern is tilted with respect to the multiviewing system's central axis.

Recently, work has been done to assess the reliability of the flaw reconstruction method as a function of the aperture size and signal-to-noise ratio of the backscatter waveform data [1]. In particular, much attention has been paid to flaw orientation and its effect on reconstruction fidelity [7]. Such work has shown that the acquisition of backscatter waveform data using ultrasonic transducers, (interrogations) on flaws that were tilted with respect to the interrogation perspective, resulted in reduced reliability of the reconstruction. It has been demonstrated [11] that acquiring backscatter data on a flaw around the vector normal to the surface of minimum curvature, based on an ellipsoidal model, results in better signal-to-noise ratio (SNR) [11]. The increased SNR will improve the reliability of the flaw reconstruction [11]. This maximization of the measurement SNR requires an a priori knowledge of the orientation of the flaw in the material. Flaw orientation determination requires a separate set of interrogations. The result is a three-step process for the model-based flaw reconstruction method:

1. Acquire data to determine the orientation of the flaw and to describe the vector normal to the surface of minimum curvature.

2. Acquire backscatter data from perspectives positioned around the vector normal to the surface of minimum curvature
3. Process the backscatter data with the flaw reconstruction routines.

Research has shown [11] that the flaw orientation information may be deduced from the angular dependency of the backscatter signal amplitude. First, the orientation of the flaw in the azimuthal plane is determined. This azimuthal plane is denoted as the X'-Y' plane and is illustrated in Figure 2 [9, 11, 12]. Next, the angular tilt of

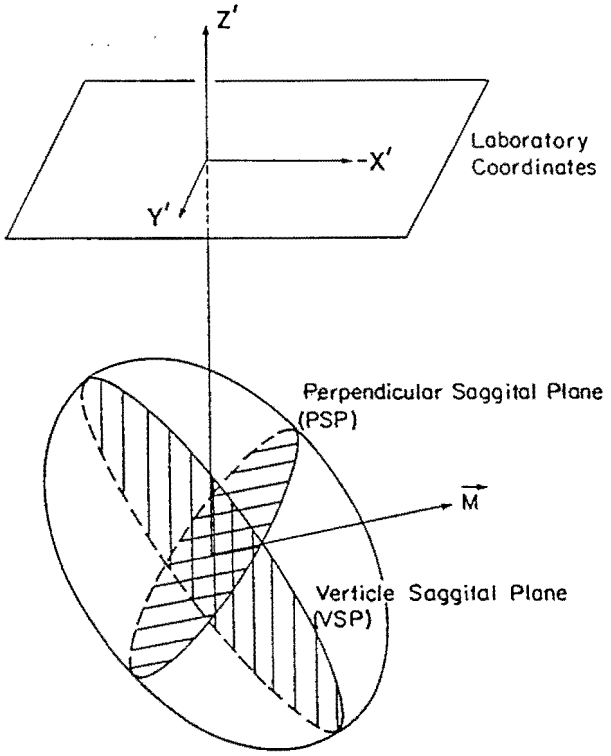

Figure 2. Laboratory Coordinate System

the flaw with respect to the Z' plane is determined. Once the flaw's orientation has been measured, a new set of coordinate axes, X-Y-Z, are defined. Figure 3 shows the definition of the polar orientation and the new coordinate axis system. From this information, a data acquisition pattern may be defined for flaw reconstruction which will provide the optimal signal-to-noise ratio and will result in improved reconstruction reliability.

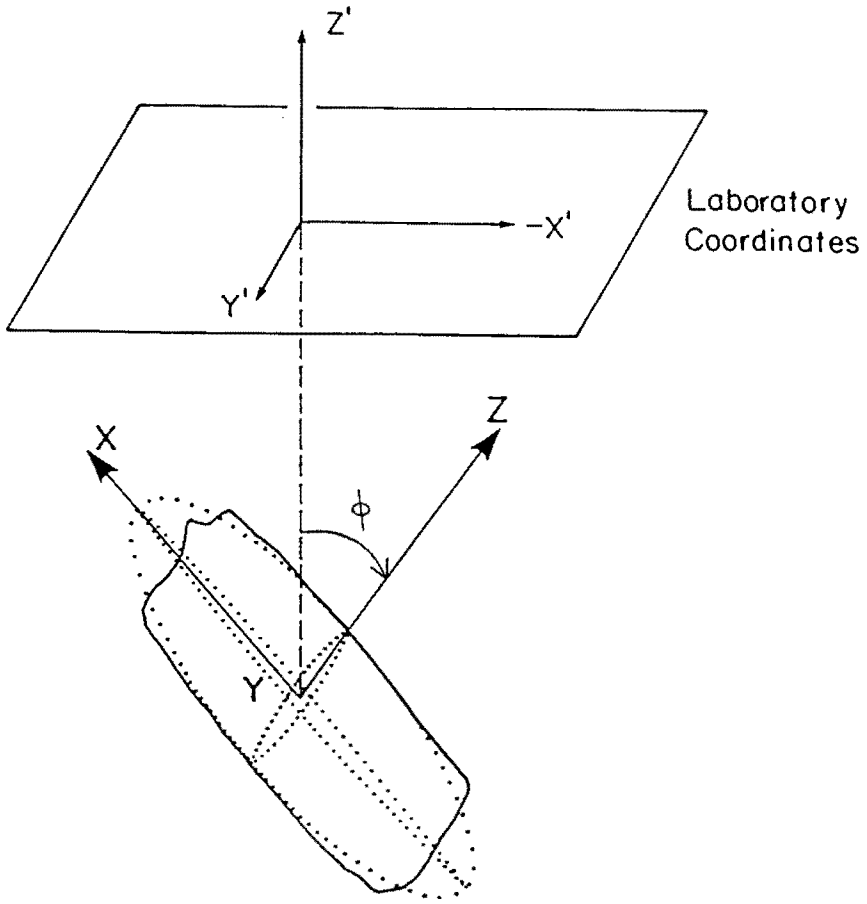

Figure 3. Polar Orientation and Coordinate Axes of the Flaw

The research work presented here involves the design and implementation of automated scan processes for determination of flaw orientation as well as the development of the data acquisition pattern to be used with the flaw reconstruction routines. The scans developed were designed to be used with an automated multiviewing ultrasonic system.

B. Research Objectives

1. To derive the equations necessary to describe the positions in three-dimensional space of a transducer used to interrogate a flaw from a particular perspective. For each transducer, this position description contains both the azimuthal and polar angles and the radial and axial positions.

2. To design a scan strategy to be used in determining the azimuthal orientation of a flaw within a material, and thus establish the orientation of the Vertical Saggital Plane (VSP) [11] based on backscatter amplitude. This VSP contains the vector that describes the azimuthal orientation for the flaw and the Z′ axis.

3. To design a scan strategy for determination of the polar orientation of a flaw that is based on backscatter amplitude.

4. To determine the vector normal to the surface of minimum curvature for a flaw modeled as an ellipsoid. This vector orients the data acquisition pattern to be used with the flaw reconstruction routines.

5. To develop the geometry and subsequent equations for a third scan which is in a plane containing a vector that is both normal to the surface of minimum curvature for the flaw and orthogonal with the VSP. This plane is called the Perpendicular Saggital Plane (PSP) [11].

6. To design and implement the software needed to accomplish the azimuthal and polar scans and to create a table of transducer positions required for the data acquisition pattern used with the reconstruction routines.

7. To use these procedures, called scan plans, to acquire data on several known flaws and then validate the scan designs and associated software.

A detailed explanation of the three scan plans is given and the solution for each is described. Appendices are included to provide background information such as the multiviewing system description. The actual software source code is not included here, but algorithm descriptions for each program are provided. The source code is included in a report filed with the NDE center.

C. Thesis Organization

This thesis is organized into sections that address each of the tasks described. Section II is an overview of the angular scans needed to attain the flaw orientation information. Section III gives

the derivation of the equations needed to describe the positions of both the multiviewing system and the individual transducers needed to interrogate a flaw from the perspectives described earlier. Section IV explains the development of the scan plans used to perform the azimuthal, polar, and PSP scans. Section V is devoted to the final data acquisition pattern and its development. Section VI is an explanation of the software algorithms. Section VII provides results of the azimuthal and polar scans performed on several known flaws.

An appendix is provided that describes the 1-D inverse Born approximation that is used for the flaw reconstruction. It also gives a description of the measurement model that extracts the absolute scattering amplitude for the flaw as required by the Born approximation. A second appendix describes the automated multiviewing ultrasonic system.

II. ANGULAR SCAN CONCEPT

As explained in the introduction, the angular dependency of the backscatter signal amplitude can be used to deduce the orientation of a flaw in a given material. Utilizing this dependency, a series of backscatter data acquisitions have been defined called "angular scans" [11]. The angular scan concept involves two separate data acquisition sequences, called scans. The output of each sequence provides a different piece of information about a flaw's orientation.

The first scan, an azimuthal scan, defines the azimuthal orientation of the Vertical Saggital Plane (VSP). This determination of the VSP is based on an ellipsoidal model for the flaw and assumes that the flaw has axial symmetry. Peak-to-peak backscatter amplitude vs azimuthal angle for the entire 360^{o} azimuthal plane is acquired for several polar angles of interrogation. The flaw is interrogated at several polar angles to improve the statistical reliability of the result. The backscatter amplitude will peak as the azimuthal angle of interrogation coincides with the VSP for the flaw, which corresponds to one of the flaw's semiaxes [11]. A plot is made of peak-to-peak amplitude vs azimuthal angle for each polar angle. By scanning several polar angles the azimuthal orientation can be determined. Figure 4A shows the results of a computer simulated azimuthal scan on a tilted, prolate-shaped flaw. As can be seen from Figure 4A, the backscatter amplitude reaches a maximum, for each polar angle of interrogation, when a particular azimuthal angle is approached. This

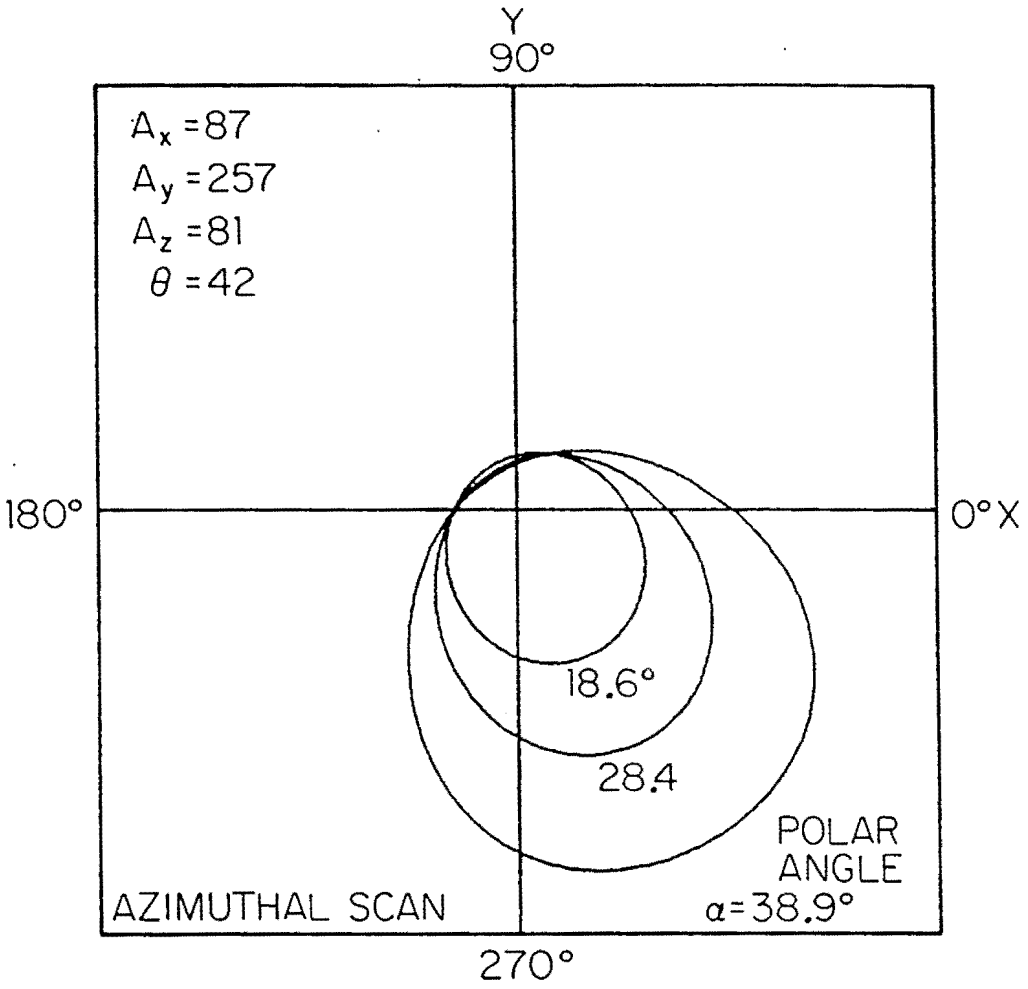

Figure 4A. Computer Simulation of an Azimuthal Scan

corresponds to the azimuthal orientation of the flaw. Figure 4A indicates an orientation of the flaw in the azimuthal plane of 315°. Figure 4B is experimental data [11] acquired on an oblate spheroidal void in titanium.

The azimuthal orientation describes the direction of the VSP. The VSP is coincident with the azimuthal orientation, contains the Z' axis, and contains a semi-axis of the flaw, assuming axial symmetry

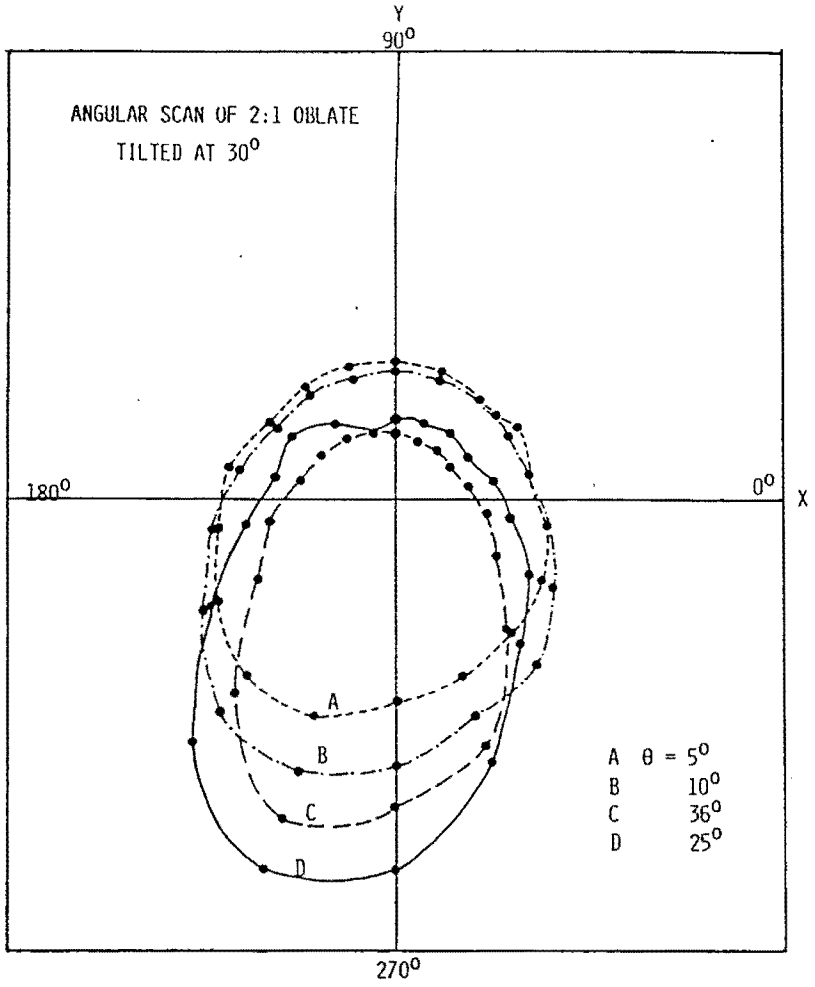

Figure 4B. Azimuthal Scan of an Oblate Spheroidal Void in Titanium

for the flaw. This plane bisects the flaw and contains the vector normal to the surface of minimum curvature; based on an ellipsoidal flaw model.

The second scan, a polar scan, is an interrogation of the flaw at many polar angles along the VSP. Backscatter data are acquired from polar angles of -90° to $+90^{\circ}$, with respect to the Z' axis, at the given azimuthal orientation. Since the backscatter amplitude is

proportional to the angular tilt of the flaw with respect to the interrogation angle [11], the backscatter amplitude will reach a maximum as the scan approaches the polar orientation of the flaw. Once the data are acquired, a plot is made of peak-to-peak amplitude vs polar angle. The plots in Figures 5A and 5B are examples of polar scan results. Figure 5A is a computer simulation of a 45° polar orientation demonstrating the peak-to-peak backscatter amplitude vs polar angle. Figure 5B is a plot of experimental polar scan data [11] acquired on a wire segment inclusion sample. The figure shows a maximum, and thus a polar orientation at, 40°.

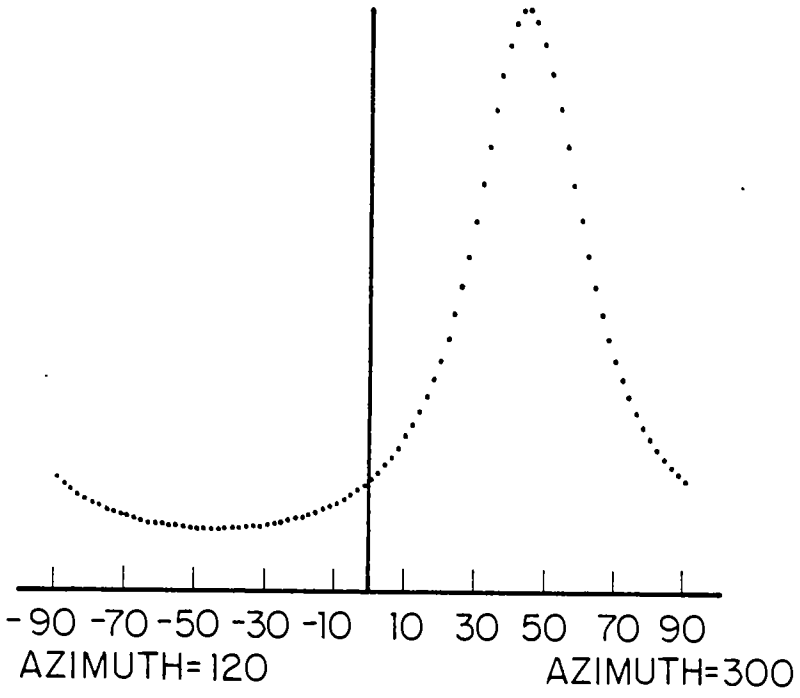

Figure 5A. Computer Simulation of a Polar Scan

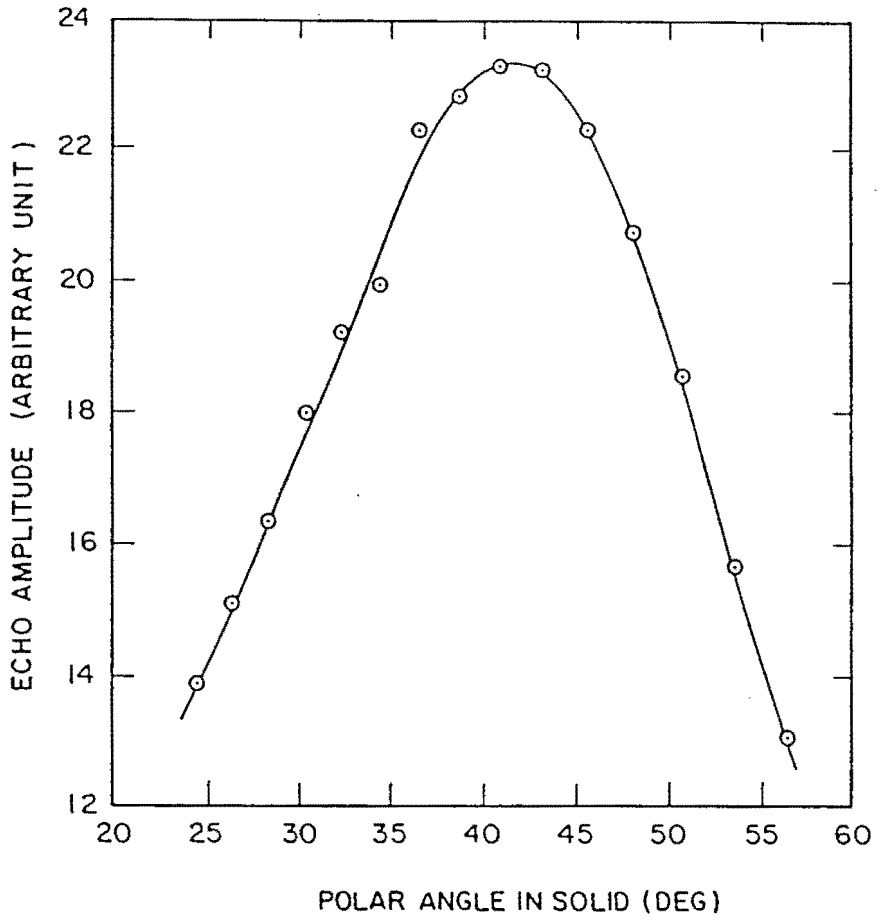

Figure 5B. Polar Scan on a Wire Segment Inclusion in Plastic

Using the results from the azimuthal and polar scans, a vector is defined coincident with the polar orientation and in the VSP. This vector is considered normal to the surface of minumum curvature for the flaw, based on an ellipsoidal model, and will be used to describe the center aperture of the data acquisition pattern used with the flaw reconstruction routines. Once the normal vector has been defined, a new set of coordinate axes are created with the normal vector as the Z

axis (see Figure 2 [9, 11, 12]). The X′ and Y′ axes are translated to the X and Y axes, with the X axis lying in the VSP. The XZ plane is the VSP, and the YZ plane is the Perpendicular Saggital Plane (PSP) which bisects the flaw, is orthogonal with the VSP, and contains the vector normal to the surface of minimum curvature (the Z axis).

By scanning along the PSP, it may be possible to gain information about the general shape of the flaw. If the flaw being interrogated was prolate in nature, the radius of curvature should remain fairly constant as the flaw is interrogated in the PSP [11]. If the flaw is oblate, one expects the backscatter amplitude to fall off as the interrogation perspective is moved from its 0° position, the Z axis, in the PSP [11]. Figures 6A and 6B are computer simulations of PSP scans for the two cases mentioned above [11]. Experimental data for the PSP scans was not available, but the PSP scan software routines developed through this research work will be used to perform PSP scans in the future. The plot of data acquired from a PSP scan will provide definite shape information only if the overall shape of the flaw is oblate or prolate. Such information may be used in future work to constrain the flaw reconstruction algorithms to the general shape information gained from this PSP scan.

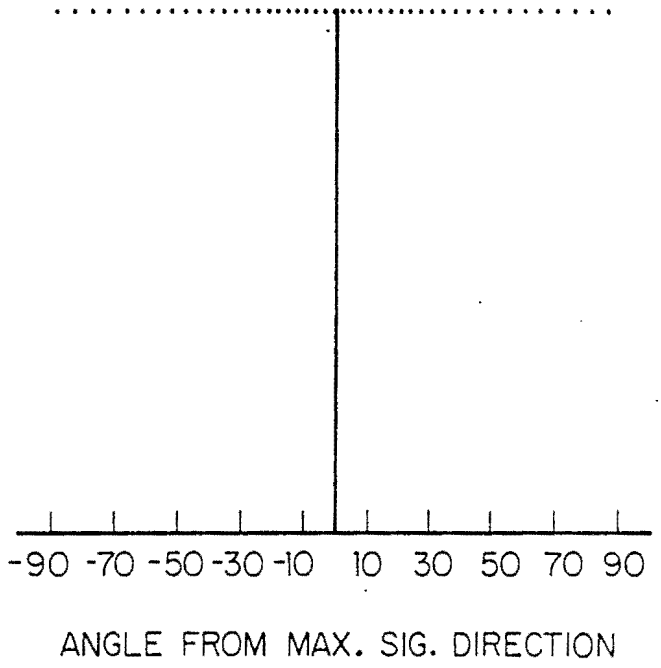

Figure 6A. Computer Simulation of PSP Scan on Prolate

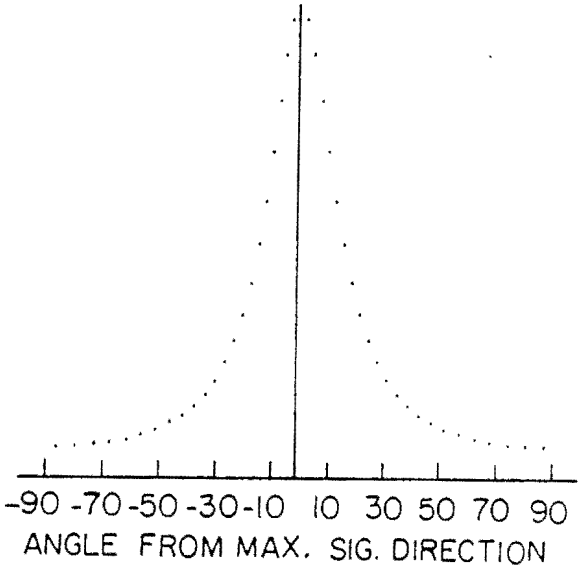

Figure 6B. Computer Simulation of PSP Scan on Oblate

III. TRANSDUCER POSITIONING

Before a discussion of the development of the scan plans is appropriate, some information about the multiviewing ultrasonic transducer system should be presented. Refer to Appendix B for this information. The entire multiviewing system may be moved within the X'-Y'-Z' space. The entire system may also be rotated about its central axis. The X'-Y' freedom allows the central axis of the multiviewing system to be positioned normally over the flaw and the freedom along the Z' axis allows for initial setting of the acoustic wave propagation time.

Since the ultrasonic interrogation is performed in an elastic medium [4, 13, 14], the principles of geometric optics [11] apply and are used to determine the transducer position in the X'-Y'-Z' space necesary to interrogate a flaw from a particular angle in the solid. Figure 7 is a view of a sample with a flaw seen looking down the Y' axis onto the X'-Y' plane, with the Z' axis over the flaw. In order to interrogate the flaw in Figure 7 from some angle β with respect to the Z' axis, the transducer must be positioned at an angle α in the water such that α and β are related by Snell's law:

$$V_m \mathrm{Sin}\alpha = V_w \mathrm{Sin}\beta \qquad (1)$$

where V_m is the velocity of the acoustic wave in the solid, and V_w is the velocity of the acoustic wave in water.

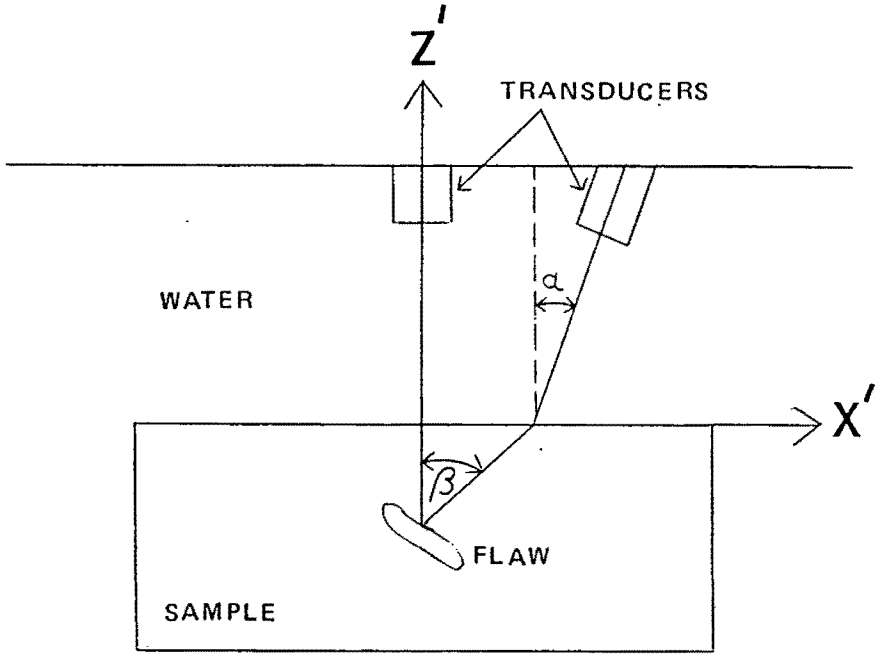

Figure 7. Flaw Interrogation Angles

We solve equation (1) for α, the angle the transducer must make with the Z′ axis in the water in order to interrogate the flaw at an angle β in the solid:

$$\alpha = \mathrm{Sin}^{-1}[(V_w/V_m)\mathrm{Sin}\beta] \qquad (2)$$

With the angular position of the transducer defined, the radial and axial transducer positions may be determined. Figure 8 shows two transducers focused on a flaw. One transducer is normal to the sample surface with its axis coincident with the Z′ axis. The other transducer is at an angle β to the Z′ axis in the solid. To determine the

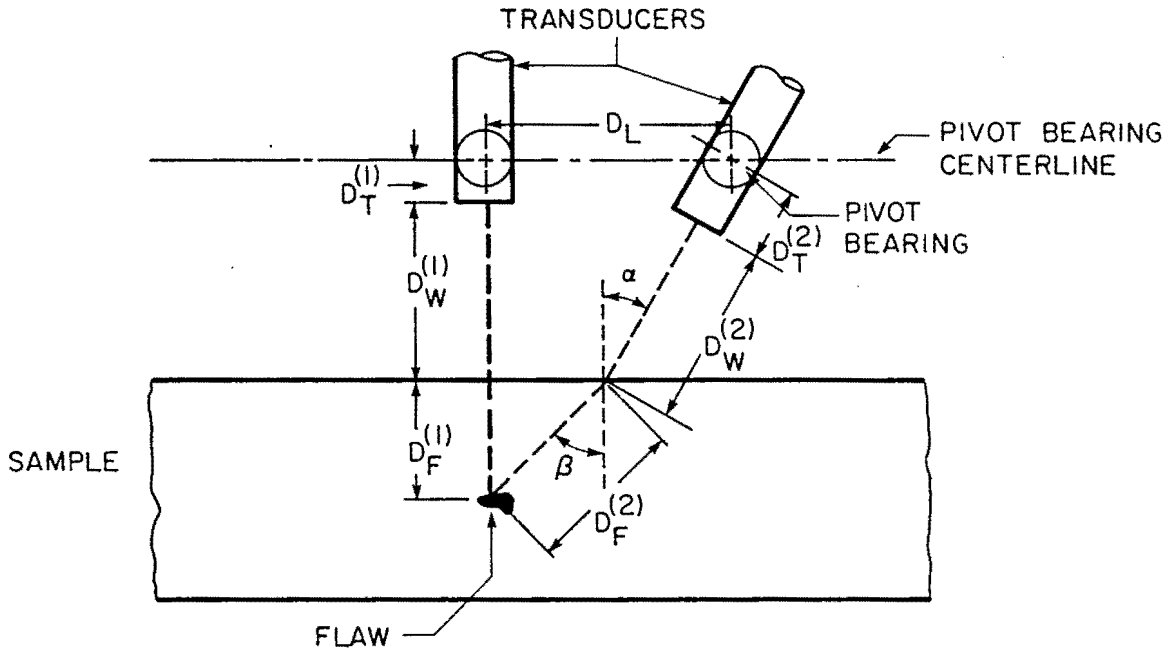

$$\alpha = \text{SIN}^{-1}\left\{V_W\left[\text{SIN}(\beta)\right] / V_M\right\}$$

$$D_L = D_F^{(1)}\left[\text{TAN}(\beta)\right] + \left[D_W^{(1)} + D_T^{(1)}\right]\left[\text{TAN}(\alpha)\right]$$

$$D_T^{(2)} = \left(D_W^{(1)} + D_T^{(1)}\right) / \text{COS}(\alpha) - D_W^{(2)}$$

V_W = acoustic velocity in water

V_M = acoustic velocity in sample host material

Figure 8. Transducer Focusing Equations

radial and axial positions for the transducer at angle α, a reference transducer is placed normal to the sample surface and coincident with the Z' axis. This transducer is placed at an axial distance just far enough from the surface of the sample to place the flaw in the transducer's far field. Work done with ultrasonic transducers modeled as piston source radiators [10] has shown that the pressure of the acoustic wave is dependent on its wavelength, the distance travelled, and the mean radius of the wave at the transducer surface. Calculations are made to find the total distance the transducer must be above the flaw in order to place the flaw in the transducer's far field [1, 2]. Then the distance that the transducer must be above the surface of the sample is computed ($D_w^{(1)}$), assuming the flaw's depth is known.

From the relationship between the wavelength, distance, and the mean radius of the acoustic wave [15], the equation for the initial transducer distance in the water needed to place the flaw in the transducer's far field is:

$$D_w^{(1)} = [fa^2/2 - D_F^{(1)}V_m]/V_w \qquad (3)$$

where $D_w^{(1)}$ is the transducer's distance above the sample surface, f is the highest frequency of operation, a is the ultrasonic wave radius at the transducer face, $D_F^{(1)}$ is the depth of the flaw, and V_m and V_w are the wave velocities in the solid and in the water respectively.

This equation defines the distance necessary to place the flaw in the transducer's far field. Far field placement is advantageous because near field placement may result in nulls in the frequency spectrum. Since the 1-D inverse Born approximation uses frequency domain information, such nulls are unacceptable. Frequency spectrum nulls can result in erroneous radius estimates (see Appendix A). Also, a flaw at a null would go undetected.

Once this distance, $D_w^{(1)}$, has been determined, the total wave propagation time, from the surface of the transducer to the flaw, is computed:

$$T_i = D_w^{(1)}/V_w + D_F^{(1)}/V_m \qquad \text{where } T_i \text{ is the acoustic wave propagation time.} \qquad (4)$$

Propagation time equalization is important because the digitizer used for data acquisition has a narrow time window. On initial set up, the digitizer's time window is adjusted so it contains the complete backscatter waveform from the transducer. By using propagation time equalization for interrogation angles other that 0°, we insure that the backscatter waveform lies within the narrow time window. The acoustic wave propagation time is used to position a transducer such that the flaw will be in the far field. Acoustic wave propagation time equalization is accomplished by positioning the transducers so that all the propagation times are equal to T_i. This insures that the flaw will be in the far field of the transducer and that the propagation time for any transducer will be the same.

Now the equations for radial and axial position can be derived. To begin, the initial position for a transducer normal to the surface of the sample, and coincident with the Z', axis is determined. The determination of the radial and axial positions necessary for interrogation at an angle β in the solid, however, are not computed based on the surface of the transducer. What must be calculated is the necessary radial position of the transducer's pivot point and the water angle, α. Figure 8 shows this pivot point. Equation 3 is used to determine the initial distance from the surface of the sample to the surface of the transducer required to place the flaw in the transducer's far field. With the transducer in some initial axial position, the distance from the surface of the transducer to the pivot point of the transducer is determined, $D_T^{(1)}$. For all calculations and scan routines, the transducer normal to the sample surface is assumed to be in this initial axial position. The initial vertical height, of the pivot point of the transducer normal to the surface of the sample, must be $D_W^{(1)} + D_T^{(1)}$. This sum is denoted as D_V. The vertical height of the multiviewing system is not varied during an experiment, so D_V is the same for any interrogation angle. This vertical height, and the initial propagation time, T_i, computed by equation 4, determine the radial and axial positions necessary to interrogate a flaw at an angle, β. The radial distance from the Z' axis to the pivot point of a transducer, for an interrogation angle β in the solid, is a function of two distances (refer to Figure 8). One is the radial distance from the Z' axis to the point where a vector at

angle β would intersect the surface of the sample. This distance is $D_F^{(1)}\text{Tan}\beta$. The other is the radial distance from this intersection point to the pivot point of the transducer, $D_V\text{Tan}\alpha$. Realizing that $D_V = D_W^{(1)} + D_T^{(1)}$, the equation for the total radial distance from the Z' axis to the transducer's pivot point, D_L, becomes:

$$D_L = D_F^{(1)}\text{Tan}\beta + [D_W^{(1)} + D_T^{(1)}]\text{Tan}\alpha \qquad (5)$$

With the radial distance and water angle determined, the axial distance, $D_T^{(2)}$, is calculated, assuming precise on acoustic wave propagation time equalization. This axial distance is from the pivot point to the forward surface of the transducer. This distance is computed by finding the total axial distance from the surface of the sample to the pivot point, and subtracting $D_W^{(2)}$. The distance $D_W^{(2)}$ is derived from the equation for propagation time as follows:

$$T_i = D_F^{(2)}/V_m + D_W^{(2)}/V_W \qquad \text{where } T_i \text{ was calculated in equation 3.}$$

$$D_F^{(2)} = D_F^{(1)}/\text{Cos}\beta$$

$$T_i = (D_W^{(1)}/\text{Cos}\beta)/V_m + D_W^{(2)}/V_W \qquad (6)$$

$$D_W^{(2)}/V_W = T_i - (D_F^{(1)}/\text{Cos}\beta)/V_m$$

$$D_W^{(2)} = V_W[T_i - (D_F^{(1)}/\text{Cos}\beta)/V_m] \qquad (7)$$

The total distance to the pivot, along the vector described by α, is:

$$D_W^{(2)} + D_T^{(2)} = (D_W^{(1)} + D_T^{(1)})/\text{Cos}\alpha \qquad \alpha < 90^\circ \qquad (8)$$

Combining equations 7 and 8, the new axial position $D_T^{(2)}$, is:

$$D_T^{(2)} = (D_W^{(1)} + D_T^{(1)})/\text{Cos}\alpha - D_W^{(2)} \quad \text{or}$$

$$D_T^{(2)} = (D_W^{(1)} + D_T^{(1)})/\text{Cos}\alpha - V_W[T_i - (D_F^{(1)}/\text{Cos}\beta)/V_m] \qquad \alpha < 90^o \qquad (9)$$

In all cases, $D_T^{(2)} \geq D_T^{(1)}$. Figure 8 summarizes the geometry and controlling equations for determination of angular, radial, and axial positions required for a transducer to interrogate a flaw at an angle β in the solid.

IV. DEVELOPMENT OF "SCAN PLANS"

In the previous section the equations were derived that describe the positions a transducer must assume to interrogate a flaw from a particular solid angle. Using these equations, automated processes were developed to perform the scans, discussed in Section I, that utilize the multiviewing ultrasonic system. The first scan is an azimuthal scan that interrogates a flaw over the entire 360^{o} azimuthal plane for several polar angles. For flaw interrogation at small angles in the solid, the two transducers that can move completely into the multiviewing system's central axis are used (see Appendix B for details). Since these two transducers are separated by 180^{o}, the interrogation of a flaw over the entire 360^{o} azimuthal plane requires the multiviewing system to only be rotated through 180^{o}, because data are acquired from both transducers for a given polar angle. Although the two transducers are matched as closely as possible, they do not have identical responses, and a normalization factor is needed to equalize the peak-to-peak backscatter amplitudes. This will result in equal peak-to-peak amplitudes from two disimilar transducers if they interrogate a flaw from the same azimuthal and polar angle. Equalization is essential since the quality of computed results depend on the relative accuracy of peak-to-peak amplitude measurements.

In order to interrogate in the azimuthal plane, the multiviewing system is rotated about its central axis (Z' axis) through some azimuthal angle. Backscatter data from that perspective are acquired

from both transducers for each polar angle. The transducers are rotated again to a new azimuthal angle, and data are acquired again. The process is repeated until all the azimuthal plane has been covered. Smaller azimuthal rotations between data points will give more exact information but a large number of points are not needed because purpose of the scan is to give approximate orientation information only. To permit flexibility in the choice of the number of scan points it was decided to let the user specify the azimuthal spacing to be used in the scan routine. For similar reasons it was also decided to allow the user to specify which polar angles of interrogation would be used.

Once the increments for azimuthal spacing and polar angles are entered, the program calculates the radial, angular (both azimuthal and polar), and axial positions, and manipulates the multiviewing system into these positions. Data are then acquired during the automated scan for the specified pattern. At each position, the backscatter waveform is digitized and the peak-to-peak amplitude of the signal is estimated. This information is stored in an array of peak-to-peak amplitudes, indexed by the azimuthal angle for each polar angle specified.

As stated, the user specifies the azimuthal spacing for the data acquisition as well as the polar angles of interrogation. For such decisions to be made, the angles of interrogation that are possible for a given sample and flaw need to be known. In addition, the normal vertical distance from the sample surface to the transducer surface

must be known. A program was written to provide this and other information needed before performing the angular scans.

To ascertain the maximum interrogation angle possible, several factors must be considered. First, sample geometry and flaw location within the sample are determined through a series of ultrasonic scans. Given the physical dimensions of the sample, and the depth and position of the flaw, the maximum interrogation angle is computed:

$$\beta_{max} = \mathrm{Tan}^{-1}[D_o^{(1)}/D_w^{(1)}] \qquad (10)$$

where $D_o^{(1)}$ is the shortest radial distance from the flaw to the edge of the sample, and $D_w^{(1)}$ is defined in Figure 8.

Next, the physical constraints of the multiviewing ultrasonic system must be considered. Using equations 1 through 9 the radial, angular, and axial positions required to interrogate the flaw from this maximum polar angle, β_{max}, are calculated. If any of the calculated positions specified by these equations are unattainable, the value of β_{max} is decreased by a specified amount and the positions are recomputed based on this new β_{max}. This procedure repeates until the maximum attainable interrogation angle is determined. After β_{max} is determined, interrogation information is computed and printed. A typical output for this program is shown in Figure 9.

The information in Figure 9 provides the necessary normal vertical height required to place the flaw in the transducer's far field and the maximum interrogation angles (solid and water). Other information provided is the frequency used for the far field calculation and the transducer's initial axial position. The position vs

angle information in Figure 9 represents twenty divisions between 0° and β_{max}. The column headings represent the following:

SA - Solid angle of interrogation.

WA - Transducer angle in the water required to interrogate the flaw at the solid angle listed.

DVT - The change in the transducer's initial axial position necessary to achieve acoustic propagation time equalization. In the convention used, a positive number denotes a position closer to the sample.

DH - The required radial distance from the central axis to the pivot point of the transducer.

DW' - The axial distance ($D_w^{(2)}$ in Figure 8) from the surface of the sample to the surface of the transducer.

AXIAL - Absolute axial position for acoustic wave propagation time equalization.

RADIAL - Absolute radial position of transducer's pivot point.

```
TRANSDUCER INITIAL POSITION: 2.5 CM
MAXIMUM APERTURE ANGLE IS:   81.0898152245 DEGREES
MAXIMUM WATER ANGLE IS:      13.3336607774 DEGREES
VERTICLE HEIGHT TO HINGE IS: 6.97677364865 CM
FREQUENCY OF OPERATION IS:   20 MHZ
DEPTH OF FLAW IN SOLID IS:   0.58 CM
DISTANCE FROM FLAW TO EDGE:  3.6995 CM
```

SA	WA	DVT	DH	DW'	AXIAL	RADIAL
0.00	0.00	0.00	0.00	3.62	2.500	-5.698
4.05	0.95	0.00	0.16	3.62	2.501	-5.542
8.11	1.89	0.01	0.31	3.62	2.505	-5.386
12.16	2.82	0.01	0.47	3.61	2.512	-5.229
16.22	3.74	0.02	0.62	3.61	2.520	-5.073
20.27	4.64	0.03	0.78	3.61	2.532	-4.918
24.33	5.52	0.05	0.94	3.60	2.546	-4.762
28.38	6.37	0.06	1.09	3.60	2.562	-4.606
32.44	7.19	0.08	1.25	3.59	2.580	-4.449
36.49	7.98	0.10	1.41	3.58	2.601	-4.291
40.54	8.73	0.12	1.57	3.57	2.625	-4.131
44.60	9.43	0.15	1.73	3.56	2.650	-3.967
48.65	10.09	0.18	1.90	3.55	2.679	-3.797
52.71	10.70	0.21	2.08	3.53	2.712	-3.618
56.76	11.26	0.25	2.27	3.51	2.749	-3.424
60.82	11.76	0.29	2.49	3.47	2.792	-3.207
64.87	12.20	0.34	2.75	3.43	2.845	-2.953
68.93	12.58	0.41	3.06	3.38	2.913	-2.636
72.98	12.90	0.51	3.49	3.29	3.008	-2.206
77.04	13.15	0.66	4.15	3.15	3.156	-1.549
81.09	13.33	0.93	5.35	2.88	3.432	-0.345

Figure 9. Aperture Angle Interrogation Information for Scan Routines

Using the information provided in Figure 9, the azimuthal scan routine may be run. When the data acquisition for the azimuthal scan is completed, the peak-to-peak amplitude vs azimuthal angle information is written into a computer file. A polar plotting routine uses this file as input and plots the peak-to-peak amplitude vs azimuthal angle for each polar angle. From this plot, the azimuthal orientation of the flaw is estimated visually. This estimate of azimuthal orientation is used for the polar scan of the flaw.

The "scan plan" for the determination of a flaw's polar orientation involves a set of data acquisitions taken at many polar angles with a transducer coincident with the Vertical Saggital Plane (VSP). The polar scan utilizes the value of β_{max} to interrogate the flaw at solid angles from $-\beta_{max}$ to $+\beta_{max}$ in 31 equally spaced steps. To begin, the multiviewing system is rotated about its central axis until two opposing transducers are coincident with the VSP. To accomplish the scan, one of the two transducers interrogates the flaw from perspectives of $-\beta_{max}$ to 0^{o}. The other transducer interrogates the flaw at angles from $+\beta_{max}/15$ to β_{max}. At each perspective, peak-to-peak backscatter data are acquired and stored. The acquired data are sent to an X-Y plotting routine. A plot of peak-to-peak amplitude vs polar angle is made from the polar scan data. The polar angle at which the backscatter amplitude peaks is considered to be the angle of polar orientation for the flaw; based on an ellipsoidal model.

Both the azimuthal and polar scans utilize the information shown in Figure 9. These scan routines assume that the central axis of the

multiviewing system has been positioned to be coincident with the Z' axis over the flaw. It is also assumed that the system has been positioned at the vertical height required to place the flaw in the transducer's far field.

The results of the azimuthal scan describe the orientation of the VSP. This VSP contains the vector that is coincident with the flaw's azimuthal orientation, it bisects the flaw, and it contains the vector normal to the surface of minimum curvature; based on an ellipsoidal flaw model [7, 8, 11]. The results of the polar scan give an indication of the polar orientation of the flaw as well as the direction of the normal vector [11]. This normal vector describes the orientation of the Z axis for the flaw's coordinate system. The plane that is orthogonal with the VSP and contains this normal vector is the Perpendicular Saggital Plane (PSP). This plane bisects the flaw and contains one of the flaw's semi-axes; assuming an ellipsoidal flaw model. Earlier it was discussed how a scan along the PSP may provide information that will help to distinguish between prolate and oblate flaws.

Scanning in the PSP presents a particular problem since a change in angle along the PSP represents a change of both azimuthal and polar angle for a transducer, as well as radial and axial changes. In the azimuthal and polar scans, each successive data point required a translation of either polar or azimuthal angle but not both. The development of the geometry for the PSP scan follows (refer to Figures 10 through 15):

1. Define point M as the point where the normal vector (represented by the Z axis) pierces the X′-Y′ plane on the surface of the sample (Figure 10).

2. Inscribe a circle on the surface of the sample with the center where the Z′ axis pierces the X′-Y′ plane. The radius is the normal distance from the Z′ axis to point M (Figure 10).

3. Draw a tangent line to the circle at point M (Figure 10).

4. Rotate the transducer through an azimuthal angle θ about the Z′axis (Figure 11).

5. Translate the transducer radially outward to bring its pivot point coincident with the tangent line (point M′ in Figure 11).

6. Tilt the transducer through an angle ϕ' to bring it coincident with the PSP (Figure 11).

7. Translate the transducer axially along the Z axis to accomplish acoustic wave propagation time equalization.

8. Acquire backscatter data.

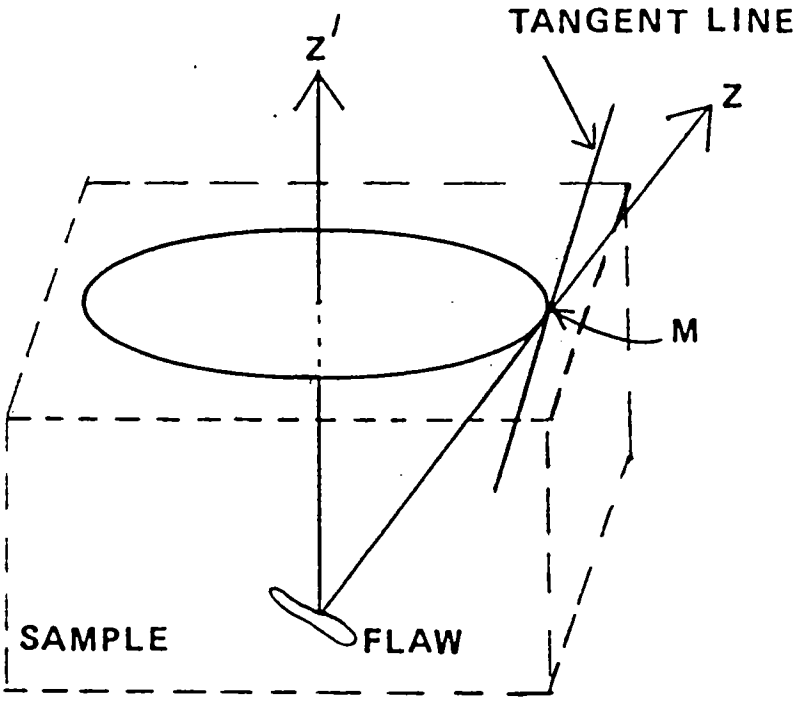

Figure 10. Tangent Line Definition

Now equations will be derived that describe the azimuthal, polar, radial, and axial translations required to position a transducer for interrogation in the PSP. Figure 12 will be used as a reference for this derivation. The line |01| represents the azimuthal orientation of the flaw. ϕ is the polar angle of the flaw and together they describe the vector normal to the surface of minimum curvature. This vector is the new Z axis (0^{o} for the PSP). The angle θ describes a translation in the azimuthal plane and ϕ' is the new polar angle required to bring the transducer back into the PSP after azimuthal translation. Point 3 is the position of the pivot point of the

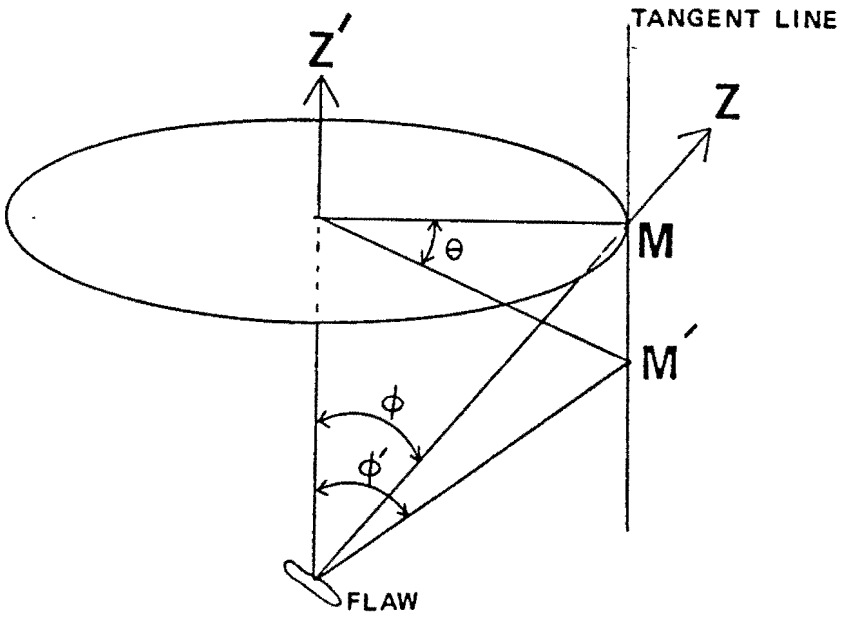

Figure 11. Translation to Bring Transducer into PSP

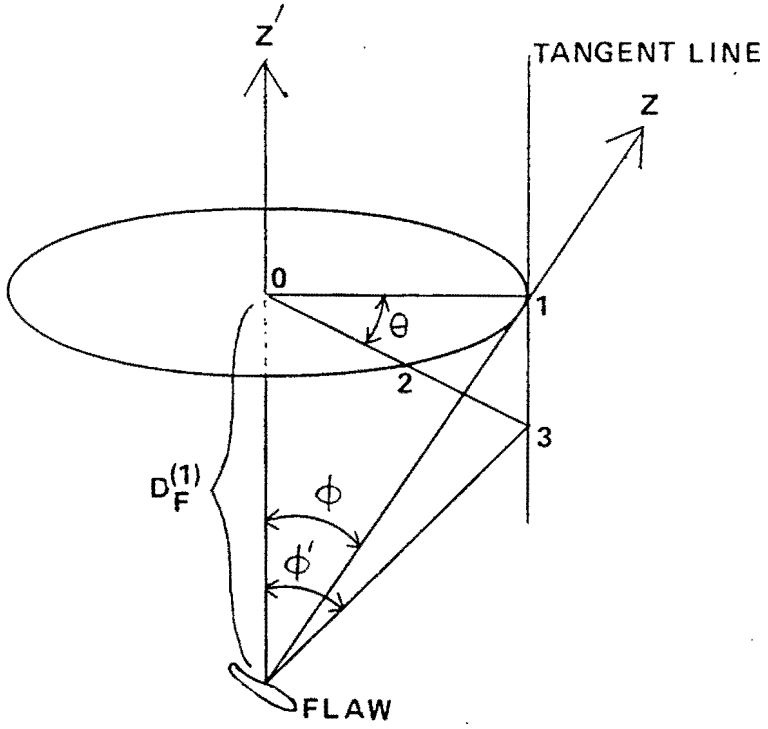

Figure 12. Interrogation in the PSP

transducer after translation in the PSP and line |23| represents the radial pull back distance for the pivot point of the transducer that is required after an azimuthal translation of θ.

$$
\begin{aligned}
|01| &= D_F^{(1)}\mathrm{Tan}\phi \\
|13| &= (D_F^{(1)}\mathrm{Tan}\phi)\mathrm{Tan}\theta \quad \text{since } |13| \text{ is normal to } |01| \text{ by definition.} \qquad (11)\\
|03| &= (D_F^{(1)}\mathrm{Tan}\phi)/\mathrm{Cos}\theta \quad |01| = |02| \\
|23| &= (D_F^{(1)}\mathrm{Tan}\phi)/\mathrm{Cos}\theta - D_F^{(1)}\mathrm{Tan}\phi \\
&= D_F^{(1)}\mathrm{Tan}\phi(1/\mathrm{Cos}\theta - 1) \qquad (12)\\
\mathrm{Tan}\phi' &= (D_F^{(1)}\mathrm{Tan}\phi/\mathrm{Cos}\theta)/D_F^{(1)} \\
&= \mathrm{Tan}\phi/\mathrm{Cos}\theta \\
\phi' &= \mathrm{Tan}^{-1}[\mathrm{Tan}\phi/\mathrm{Cos}\theta] \qquad (13)
\end{aligned}
$$

This new polar angle, ϕ', is the polar angle required to bring the transducer coincident with the PSP given the azimuthal translation. What follows is verification that the radial and angular translations shown do produce a translation in the PSP. The equations and computations given will be in the solid only. Once the angle is verified, the derivation of the positions necessary for the transducer in the water will be shown.

Figure 13 shows the side view of the flaw looking down the Y′ axis. This describes the direction of the flaw and the PSP normal.

Direction of PSP normal is: $(\sin\phi, 0, \cos\phi)$ (A)

Direction of flaw is: $(-\cos\phi, 0, \sin\phi)$ (B)

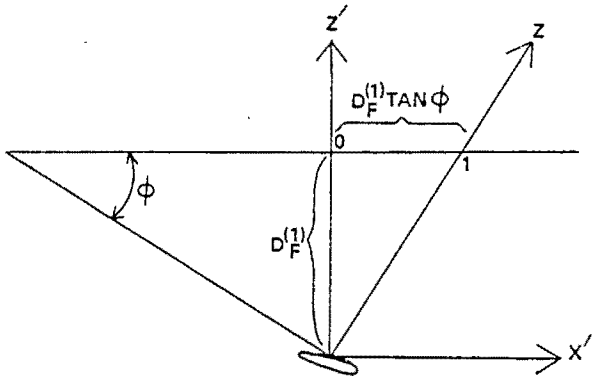

Y′ axis into page
$D_F^{(1)}$ = depth of flaw

Flaw lies in X-Y plane

Figure 13. Side View of Flaw Looking Down the Y′ Axis

Figure 14 shows the transducer direction after the azimuthal translation but before the radial translation to point 3.

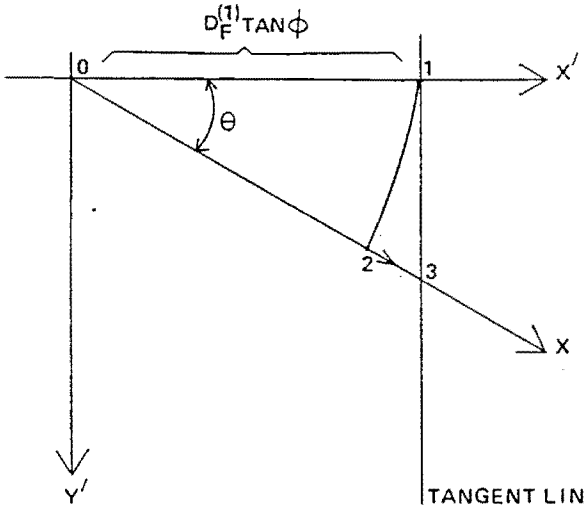

1) At position 1, transducer is coincident with normal vector, Z′ axis, and is in the PSP.

2) At position 2, transducer direction is: $(\sin\phi\cos\theta, \sin\phi\sin\theta, \cos\phi)$

Figure 14. Top View of Flaw Looking Down the Z′ Axis

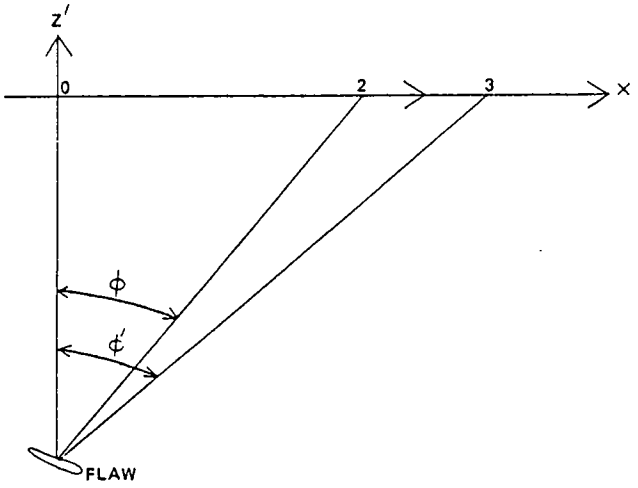

1) |23| is the radial pullback distance.

2) $|03| = [(D_F^{(1)}\text{Tan}\phi) + (D_F^{(1)}\text{Tan}\phi\text{Tan}\theta)^2]^{1/2}$

3) Pullback distance is: $D_F^{(1)}\text{Tan}\phi(1/\text{Cos}\theta - 1)$

Figure 15. The X-Z′ View of the Flaw

After the tilt, the new polar angle is ϕ'.

$$\text{Tan}\phi' = (D_F^{(1)}\text{Tan}\phi/\text{Cos}\theta)/D_F^{(1)}$$

$$= \text{Tan}\phi/\text{Cos}\theta$$

The final direction of interrogation for the transducer is:

$(\text{Sin}\phi'\text{Cos}\theta, \text{Sin}\phi'\text{Sin}\theta, \text{Cos}\phi')$.

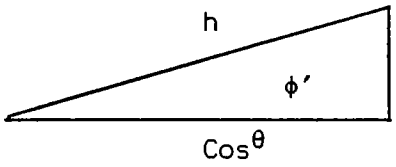

Tanϕ

$$h = (\text{Tan}^2\phi + \text{Cos}^2\theta)^{1/2}$$

$$\text{Sin}^{\phi'} = \text{Tan}^{\phi}/h$$

$$\text{Cos}^{\phi'} = \text{Cos}^{\theta}/h$$

Final direction is $(\text{Tan}\phi\text{Cos}\theta/h, \text{Tan}\phi\text{Sin}\theta/h, \text{Cos}\theta/h)$ (C). To check if the final direction is in the PSP, we look at the dot product of B and C: $B \cdot C = \sum_i b_i c_i$ where $B = b_1 i + b_2 j + b_3 k$ and $C = c_1 i + c_2 j + c_3 k$

$$= -\text{Sin}\phi\text{Cos}\theta/h + \text{Sin}\phi\text{Cos}\theta/h = 0$$

Since the original position was in the VSP and the PSP, and the new direction is orthogonal with the VSP, the final direction lies in the PSP.

Now the calculations will be made to determine the angle between the original direction (PSP normal) and the final direction. Let this angle be ζ.

$$\text{Cos}\zeta = (A \cdot C)/|A||C| \tag{14}$$

$$\begin{aligned} A \cdot C &= \text{Sin}^2\phi(\text{Cos}\theta/h)\text{Cos}\phi + \text{Cos}\phi\text{Cos}\theta/h \\ &= 1/h[\text{Cos}\theta/\text{Cos}\phi] \end{aligned} \tag{15}$$

$$\begin{aligned} |A| &= 1 \\ |C| &= 1/h[\text{Tan}^2\phi\text{Cos}^2\theta + \text{Tan}^2\phi\text{Sin}^2\theta + \text{Cos}^2\theta]^{1/2} \\ &= 1/h[\text{Tan}^2\phi + \text{Cos}^2\theta]^{1/2} \end{aligned}$$

$$\begin{aligned} \text{So: } \text{Cos}\zeta &= [1/h(\text{Cos}\theta/\text{Cos}\phi)]/[1/h(\text{Tan}^2\phi + \text{Cos}^2\theta)^{1/2}] \\ &= \text{Cos}\theta/[\text{Cos}\phi(\text{Tan}^2\phi + \text{Cos}^2\theta)^{1/2}] \\ \zeta &= \text{Cos}^{-1}\{\text{Cos}\theta/[\text{Cos}\phi(\text{Tan}^2\phi + \text{Cos}^2\theta)^{1/2}]\} \end{aligned} \tag{16}$$

To see if equation 16 is valid for all angles, we will test the following two limiting cases:

1. When $\theta = 90^\circ$ the new polar angle ϕ' should be 90°, independent of ϕ.

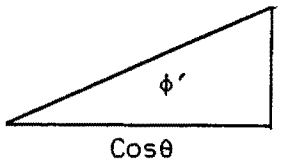

If $\theta = 90^{o}$, $\cos\theta = 0^{o}$ and $\phi' = 90^{o}$

2. When $\theta = 90^{o}$, ζ should be 90^{o}, independent of ϕ.

$$\cos\zeta = \cos\theta/[\cos\phi(\tan^2\phi + \cos^2\theta)^{1/2}]$$

if $\theta = 90^{o}$, $\cos\theta = 0^{o}$ and $\zeta = 90^{o}$

With the verification complete, we have the equation to describe an angle in the PSP in terms of the polar orientation of the flaw and the azimuthal translation:

$$\zeta = \cos^{-1}\{\cos\theta/[\cos\phi(\tan^2\phi + \cos^2\theta)^{1/2}]\}$$

where ζ = interrogation angle in the PSP.
ϕ = polar orientation of the flaw.
θ = azimuthal rotation of multiview system about the Z′ axis.

This equation defines the interrogation angle in the PSP given the polar orientation of the flaw and some azimuthal rotation of the system. However, in order to create an automated process for scanning in the PSP, what is needed is an equation that calculates the azimuthal rotation necessary to interrogate the flaw at an angle ζ in the PSP. The derivation of this equation is:

$$\cos\zeta = \cos\theta/[\cos\phi(\tan^2\phi + \cos^2\theta)^{1/2}]$$

$$\cos\theta = \cos\zeta\cos\phi(\tan^2\phi + \cos^2\theta)^{1/2}$$

$$\cos^2\theta = \cos^2\zeta\cos^2\phi(\tan^2\phi + \cos^2\theta)$$

$$\cos^2\theta(1 - \cos^2\phi\cos^2\zeta) = \cos^2\zeta\cos^2\phi\tan^2\phi$$

$$\cos^2\theta = \cos^2\zeta\sin^2\phi/(1 - \cos^2\zeta\cos^2\phi)$$

$$\theta = \pm \cos^{-1}\{[\cos^2\zeta\sin^2\phi/(1 - \cos^2\zeta\cos^2\phi)]^{1/2}\} \qquad (17)$$

This equation for θ describes the change in azimuthal rotation necessary to achieve interrogation of a flaw at an angle ζ in the PSP. To recap, the controlling equations for the PSP scan are:

1) The change in azimuthal angle, θ, required for an interrogation in the PSP at angle ζ:

   $$\theta = \pm \cos^{-1}\{[\cos^2\zeta\sin^2\phi/(1 - \cos^2\zeta\cos^2\phi)]^{1/2}\}$$

   where ϕ is the polar orientation of the flaw and ζ is the desired angle in the PSP.

2) Change in radial distance needed to interrogate a flaw at an angle ζ in the PSP is:

   $$D_F^{(1)}\tan\phi(1/\cos\theta - 1) \qquad (18)$$

3) Total radial distance from the Z′ axis to the pivot point of the transducer for an interrogation in the PSP at angle ζ:

   $$D_F^{(1)}\tan\phi/\cos\theta \qquad (19)$$

4) Polar angle for the transducer is:

   $$\phi' = \tan^{-1}[\tan\phi/\cos\theta] \qquad (20)$$

Once these distances and angles have been determined, the axial

change necessary to achieve time equalization is computed. The PSP scan routine will utilize equations 17 through 20 to position the transducer for interrogating a flaw at perspectives along the PSP. The scan routine will interrogate the flaw at angles up to the maximum attainable angle in the PSP. The maximum PSP angle is computed using equation 20. In the first program discussed, the maximum interrogation angle was calculated, β_{max}. This maximum interrogation angle is also the maximum ϕ' available, or $\phi'_{max} = \beta_{max}$. If the transducer were interrogating a flaw at an angle ϕ'_{max}, the azimuthal angle, θ_{max}, associated with ϕ'max would be:

$$\phi'_{max} = \mathrm{Tan}^{-1}[\mathrm{Tan}\phi/\mathrm{Cos}\theta_{max}] \qquad \phi = \text{polar orientation} \tag{21}$$

$$\mathrm{Tan}\phi'_{max} = \mathrm{Tan}\phi/\mathrm{Cos}\theta_{max}$$

$$\theta_{max} = \mathrm{Cos}^{-1}[\mathrm{Tan}\phi/\mathrm{Tan}\phi'_{max}]$$

$$\theta_{max} = \mathrm{Cos}^{-1}[\mathrm{Tan}\phi/\mathrm{Tan}\beta_{max}] \tag{22}$$

Using this value of θ_{max}, The maximum ζ may be found from equation 16:

$$\zeta_{max} = \mathrm{Cos}^{-1}[\mathrm{Cos}\theta_{max}/\mathrm{Cos}\phi(\mathrm{Tan}^2\phi + \mathrm{Cos}^2\theta_{max})^{1/2}] \tag{23}$$

The equations above describe the interrogation angles and positions inside the solid. For the PSP scan routine, however, the equations that describe the transducer's movements in the water are needed. Equation 1 is used to derive these angles and positions:

$$1)\quad \phi'_{water} = \mathrm{Sin}^{-1}[(V_w/V_m)\mathrm{Sin}\phi'_{solid}]$$

$$= \mathrm{Sin}^{-1}\{(V_w/V_m)\mathrm{Sin}[\mathrm{Tan}^{-1}(\mathrm{Tan}\phi/\mathrm{Cos}\theta)]\} \tag{24}$$

where V_w is the velocity of the acoustic wave in the water and V_m is the velocity of the wave in the solid.

2) Total radial distance in the water from the Z′ axis:

$$D_H = D_F^{(1)}\mathrm{Tan}\phi'_{solid}/\mathrm{Cos}\theta + D_V\mathrm{Tan}\phi'_{water}$$

$$= D_F^{(1)}\mathrm{Tan}\phi'_{solid}/[\mathrm{Cos}^2\zeta\mathrm{Sin}^2\phi/(1-\mathrm{Cos}^2\zeta\mathrm{Cos}^2\phi)]^{1/2}$$

$$+ D_V\mathrm{Tan}\{\mathrm{Sin}^{-1}[(V_w/V_m)\mathrm{Sin}[\mathrm{Tan}^{-1}(\mathrm{Tan}\phi/\mathrm{Cos}\theta)]]\} \qquad (25)$$

where D_H is the radial distance from the Z′ axis and D_V is the vertical distance from the surface of the solid to the pivot point of the transducer.

3) θ remains the same.

From these and previous equations, calculations are made for the radial, angular, and axial positions necessary to interrogate the flaw at angles in the PSP. Computations are made for a PSP angle of ζ_{max}. If any of the positions are unattainable, the value of ζ_{max} is decreased by a preset amount and the calculations repeated. The process is continued until the largest angle in the PSP that can be achieved is found. This value of ζ_{max} will be divided into a suitable number of divisions, and a routine will interrogate the flaw from angles of $-\zeta_{max}$ to $+\zeta_{max}$. The peak-to-peak amplitude of the backscattering waveform from each perspective will be stored. After completion of the scan, an X-Y plot will be made of peak-to-peak amplitude vs PSP angle. The plot of these data gives an indication of flaw shape, either oblate or prolate.

V. FINAL DATA ACQUISITION PATTERN

Previously, azimuthal and polar scans were discussed. The results were used to determine the vector normal to the surface of minimum curvature for a flaw, based on an ellipsoidal model. This vector is used to locate the center aperture of the data acquisition pattern for the model-based flaw reconstruction routines.

In the search for a data acquisition pattern suitable for the flaw reconstruction work, three factors were considered. First, from previous work [1, 7, 9, 11, 12], it has been shown that interrogation of a flaw from thirteen independent perspectives is sufficient to provide adequate results from the best fit algorithms. Second, the acquisition pattern should require as few movements of the multiviewing system as possible. This will facilitate fast, efficient data acquisition. Third, the physical constraints of the multiviewing system must be considered. Ideally, the pattern should be conical around the vector normal to the surface of minumum curvature (the Z axis) [1, 4, 7, 9]. Figure 16 illustrates this pattern. The physical constraints of the multiviewing system, however, do not allow interrogation using such a pattern. In order to practically perform interrogations along this conical pattern, the central axis of the multiviewing system must be translated along the VSP to position the central axis coincident with the normal vector. However, if the central axis of the multiviewing system is not coincident with the Z' axis, only those two transducers lying in the VSP may interrogate the

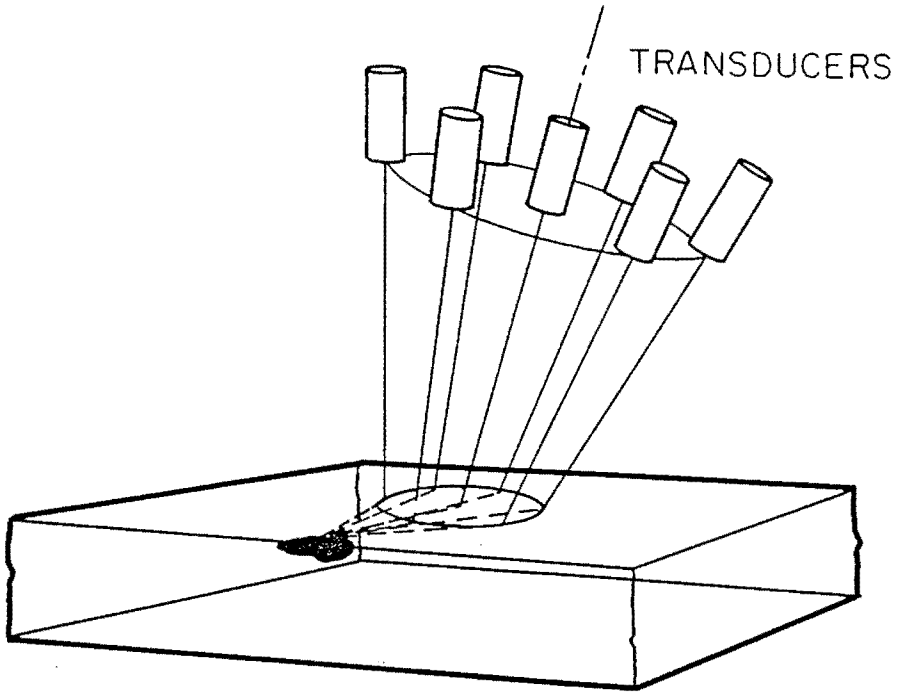

Figure 16. Ideal Conical Acquisition Pattern

flaw. Do to mechanical limitations, the transducers may only be tilted at an angle toward the system's central axis. In order for a transducer to interrogate a flaw, however, the transducer must tilt in a plane containing both the Z' axis and the pivot point of the transducer. The only way all six transducers can meet this criterion is if the central axis of the multiviewing system and the Z' axis are coincident.

In spite of these practical constraints, a pattern that provides adiquate interrogations around the normal vector was found. Figure 17

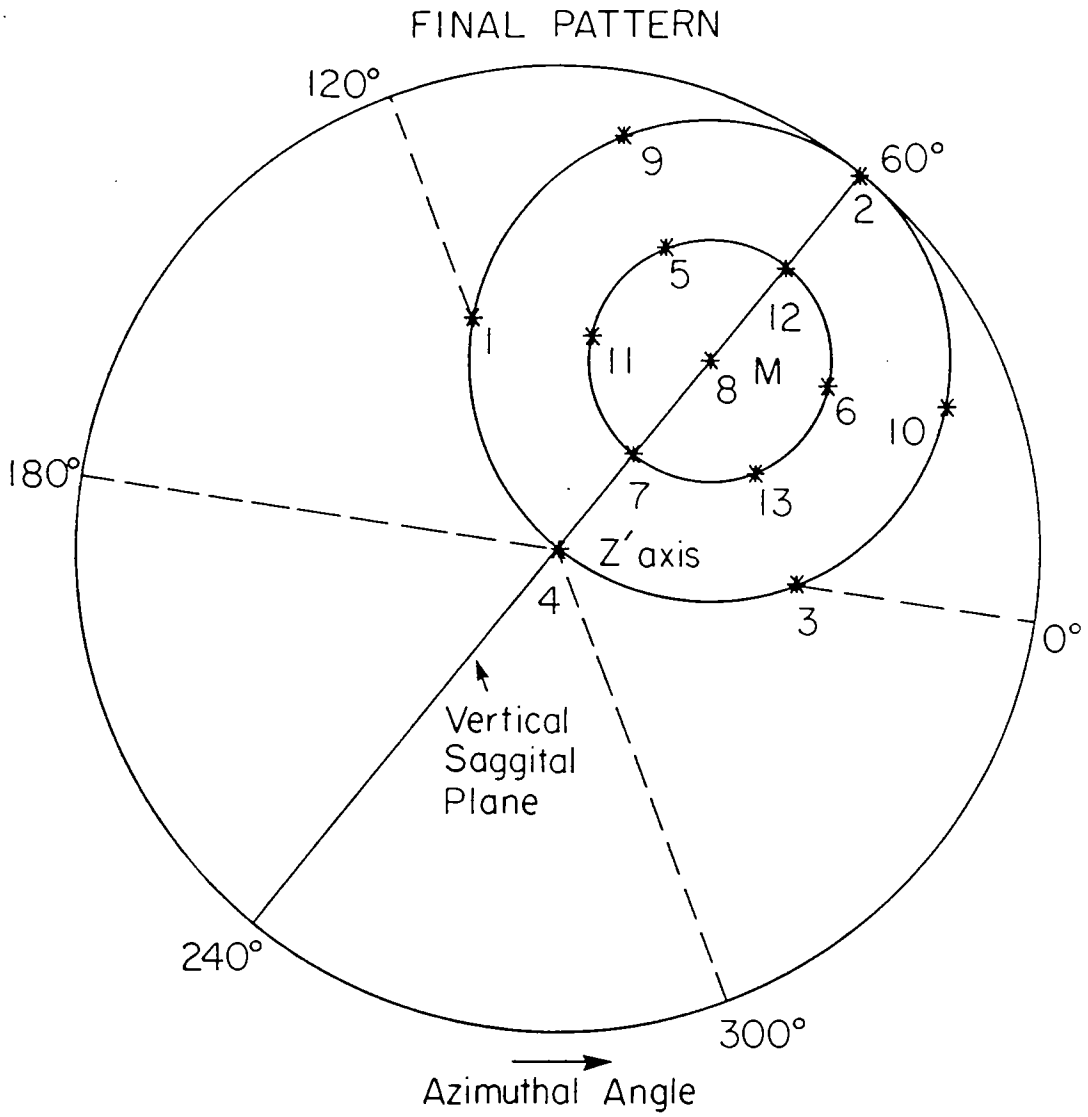

Figure 17. Data Aquisition Pattern for Flaw Reconstruction

illustrates the designed aquisition pattern. This is an azimuthal projection of the pattern onto the X′-Y′ plane. The acquisition pattern is centered around the vector normal to the surface of minimum curvature. This vector lies in the VSP. Since the direction of the VSP and the polar orientation are known at this point, they are used to create a data acquisition pattern symmetric with respect to the VSP. Since, for any situation, the orientation of the VSP is known, the equations are simplified for the transducer positioning if the interrogation perspectives are always computed with respect to the VSP. The pattern consists of acquisition points that lie on the two concentric circles (A and B) shown in Figure 17. This pattern depicts the 13 sampling positions for the acoustic waves as they penetrate the X′-Y′ plane. Point M in Figure 17 is the point where the Z axis pierces the X′-Y′ plane. The Z axis locates the center aperture for the data acquisition pattern. The pattern is made symmetric with the VSP and utilizes the perspective at the Z′ axis. To accomplish this, the radius of the outer circle, circle A, is the distance from the Z′ axis to point M. Therefore, the distance from the Z′ axis (point 4 in Figure 17) to point 2 is twice the radius of circle A. From here, the maximum interrogation angle, which is the interrogation angle for position 2, ϕ'_{max}, is computed:

$$\phi'_{max} = \mathrm{Tan}^{-1}(a/D_F^{(1)})$$

where ϕ'_{max} is the interrogation angle in the solid, a is twice the distance from the Z′ axis to point M, and $D_F^{(1)}$ is the flaw depth.

$a = 2D_F^{(1)}\mathrm{Tan}\phi$ where ϕ is the polar orientation angle.

$$\phi'_{max} = \mathrm{Tan}^{-1}[2D_F^{(1)}\mathrm{Tan}\phi/D_F^{(1)}]$$

$$= \mathrm{Tan}^{-1}(2\mathrm{Tan}\phi) \qquad (26)$$

Circles A and C in Figure 17 have an interesting correlation. The radius of circle A is one-half that of circle C. If a tangent line at point 4 is drawn to circle A it will be orthogonal to the VSP. Therefore, this represents a 90° change in angle on circle C. However, this same distance on circle A represents a 180° change. Therefore, a change of angle θ on circle A corresponds to a change of 2θ on circle C.

The actual acquisition pattern is described in terms of circular patterns of points that lie on circles A and B. The entire acquisition scheme consists of two separate sets of motions and acquisitions. The first is accomplished with transducers in positions 1, 2, 3, and 4 in Figure 17. Positions 1 and 3 are interrogations at a polar angle equal to ϕ, the polar orientation of the flaw, but at an azimuthal orientation of +/- 60° from the VSP. This is necessary, since the transducers are spaced 60° apart. This has the advantage that the azimuthal angles for these two positions are already set, and thus the polar angle of interrogation is already known. Since the transducer in position 4 is normal to the sample surface, no calculations are required for this position. The only angular calculation required (equation 26) is for the transducer at position 2. From these first four positions, the first eight data acquisitions

are taken in a combination of pulse-echo and pitch-catch. Pulse-echo backscatter waveform data are acquired at positions 1, 2, 3, and 4. Pitch-catch acquisitions are used to approximate the data from data points 5, 6, 7, and 8. Table 1 shows the pitch-catch arrangement used to approximate the data for a particular data point.

Table 1. Pitch-Catch Arrangements for First Acquisition

Data point	Pitch-catch positions (from - to)
5	1 - 2
6	2 - 3
7	3 - 1
8	4 - 2

The second set of motions and acquisitions for data points 9 through 13 are accomplished similarly. First, the multitransducer system is rotated about its central axis 30° azimuthally. This corresponds to a 60° azimuthal change on circle B. Then transducers are translated radially to positions 9 and 10. The angle of interrogation for positions 9 and 10 is then computed. Figure 18 illustrates the geometry of this calculation. Figure 18(A) is the azimuthal projection for position 10. Figure 18(B) shows the polar projection. The right triangle is formed by positions 2, 4, and 10.

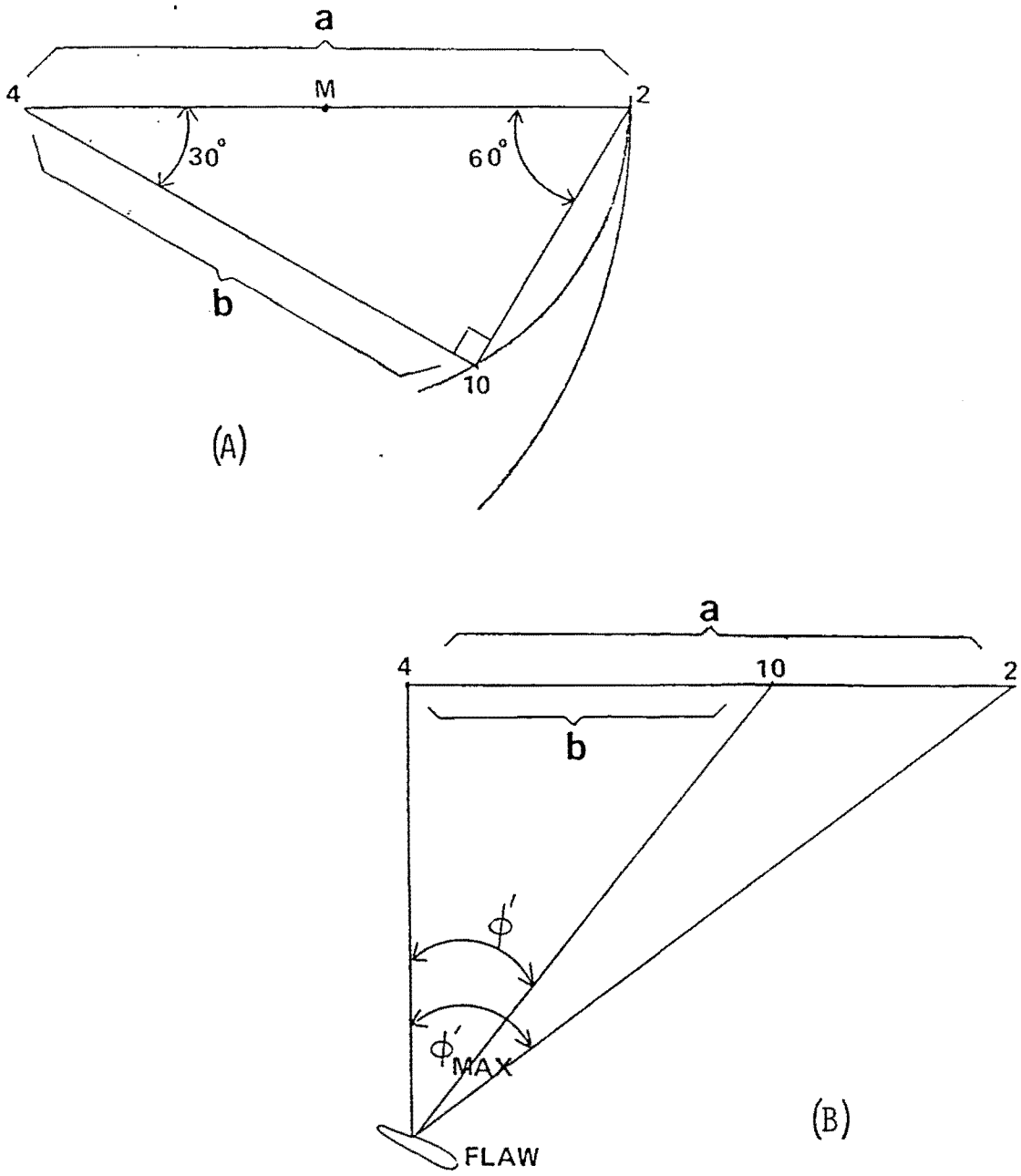

Figure 18. Angles and Distances for Second Data Aquisition

The distance b, from position 4 to 10, is:

$b = a\cos 30^{o}$ Since it was specified that the azimuthal change was 30^{o}.

The polar angle of interrogation needed for this position is:

$\phi' = \mathrm{Tan}^{-1}[a\mathrm{Cos}30^{o}/D_F^{(1)}]$ where ϕ' is the polar angle of interrogation at positions 9 and 10, $D_F^{(1)}$ is the depth of flaw defined earlier, and a is the radius of circle B.

However, $a = 2D_F^{(1)}\mathrm{Tan}\phi$ where ϕ is the polar orientation of the flaw in the solid.

Therefore:

$$\phi' = \mathrm{Tan}^{-1}[2D_F^{(1)}\mathrm{Tan}\phi\mathrm{Cos}30^{o}/D_F^{(1)}]$$

$$= \mathrm{Tan}^{-1}[2\mathrm{Cos}30^{o}\mathrm{Tan}\phi]$$

$$\phi' = \mathrm{Tan}^{-1}[\mathrm{sqrt}(3)\mathrm{Tan}\phi] \qquad (27)$$

This defines the polar angle of interrogation for positions 9 and 10. The azimuthal angle of interrogation is $+/-30^{o}$ from the VSP. Once transducers have been positioned at 9 and 10, the second set of data acquisitions are taken. Pulse-echo data are acquired at positions 9 and 10. Table 2 gives the pitch-catch arrangement for data aquisition points 11 through 13.

This data acquisition pattern allows the thirteen data points to be taken with only two sets of motions, and very few calculations. The routine is efficient and provide good backscatter data for the reconstruction routines. The equations given in this section reflect

distances and positions in the solid only. Calculations are made, for transducer positioning in the water, based on the equations derived in Section III along with the angles and distances calculated in this section.

Table 2. Pitch-Catch Arrangements for Second Acquisition

Data point	Pitch-catch positions (from - to)
11	4 - 9
12	9 - 10
13	10 - 4

The actual software implementation of this set of data acquisitions performs the calculations for all the positions and stores them in a data array. The acquisition routine then reads these positions and performs data aquisitions from the positions specified.

VI. SOFTWARE DEVELOPMENT

The software for the scan routines was written for the Tektronix 4052 graphics computer, which is the host computer for the ultrasonic scanning system. The programs were written in Basic because it is the only language that may be used with the 4052. The source code for the programs will not be given here. However, algorithms descriptions for the routines will be presented.

A. A program to Determine Possible Interrogation Angles

This program calculates and prints a table of the available interrogation angles in the solid. It uses the sample geometry and physical contraints of the multiviewing system. The printed table lists the angles of interrogation and their associated transducer positions. The program output shown in Figure 9 is intended to provide the information necessary to run the scan routines. The following algorithm description applies to the software that creates the output shown in Figure 9:

1. Read the system file of information on the sample with the flaw.
2. Enter shortest radial distance from flaw to edge of sample.

3. Calculate largest angle of interrogation possible, β_{max}, based on sample geometry.
4. Use equations 1-9 to compute the angular, radial, and axial positions necessary to interrogate the flaw at β_{max}.
5. Check to see if any of the positions calculated are unattainable. If any are, decrease β_{max} by 3^{o} and repeat step 4.
6. Divide the range from 0^{o} to β_{max} into twenty divisions and print a table of the transducer positions necessary to interrogate the flaw from each angle.

The next program executed performs the azimuthal scan.

B. A Program to Perform an Azimuthal Scan at Several Polar Angles

The azimuthal scan program makes use of the maximum interrogation angle, β_{max}, and the vertical height, D_v. Upon execution, the user is prompted to enter the number and value of all polar angles of interrogation desired. The azimuthal scan for each polar angle is performed at 10^{o} spacings. Calculations are made to determine the transducer positions necessary to interrogate the flaw at the first polar angle. The scan is achieved by first moving transducer 6 into position and acquiring backscatter data at azimuthal angles from 0^{o} to 170^{o}. Transducer 6 is then retracted and transducer 3 is positioned.

Backscatter data are then acquired from transducer 3 at azimuthal angles from 180^{o} to 350^{o}. Once the scan for the first polar angle is complete, calculations for interrogation at the next polar angle are made. The process is repeated for the remaining polar angles. The algorithm description for the azimuthal scan routine is:

1. Enter the desired number and value of polar angles of interrogation.
2. Read the data array and compute angular, radial, and axial positions required for interrogation of the flaw at the first angle specified.
3. Make sure transducer 3 is retracted.
4. Set T/R switch to transducer 6.
5. Position transducer 6 for scan.
6. Move system's X axis to 0^{o} position.
7. Acquire backscatter data.
   a. Digitize.
   b. Find peak-to-peak (p-p) value of the data.
   c. Store p-p value in system array.
8. Repeatatively execute step 7, advancing the azimuthal angle by 10^{o} until the azimuthal angle is greater than 170^{o}.
9. Retract transducer 6.
10. Set T/R switch to transducer 3.
11. Position transducer 3 for scan.
12. Move system's X axis to 0^{o} position, which places

transducer 3 at 180°.

13. Repeatatively execute step 7 by advancing the azimuthal angle by 10° until the azimuthal angle is > 350°.
14. Repeat steps 3 thru 15 for all remaining interrogation angles.
15. Write the data array of p-p amplitude vs azimuthal angle for each polar angle to computer memory.

When all scans have been completed, the polar plotting routine is executed.

C. A Polar Plot Program for Azimuthal Scan Information

The polar plotting routine takes the p-p amplitude vs azimuthal angle information for each polar angle of interrogation and creates a polar plot. All scans are put on the same plot. To begin, the program draws the outside grid for the plots and puts the labels on the plot. The next step is to determine the maximum value of the data. Once the maximum value is determined, this value is used for all plots. In order to plot the information, the p-p value vs polar angle must be converted to X and Y coordinates. A line is then drawn from each two successive sets of coordinates. This process is repeated for each polar angle of interrogation. Once the data files for the polar plots have been made, a hard copy of the plot is made.

From this plot the user visually determines the azimuthal orientation of the flaw. This line of orientation describes the VSP. This information is used in the polar scan routine. The following algorithm description applies to the polar plotting routine:

1. Create the outer grid for plots.
    a. Outer grid to run from 5% to 95% of screen, for both X and Y.
    b. Draw center grid for 0^{o}, 90^{o}, 180^{o}, and 270^{o} polar angle locations.
    c. Write in 0^{o}, 90^{o}, 180^{o}, and 270^{o} outside the grid at the proper locations.
2. Read data array.
3. Calculate X and Y coordinates for each data point.
    a. Original form is in polar coordinates
        1. p-p amplitude
        2. azimuthal angle
    b. X coordinate = p-p amplitude*COS(angle)
    c. Y coordinate = p-p amplitude*SIN(angle)
    d. Compute coordinates for polar plot for each interrogation angle. Store coordinates in arrays.
4. Draw azimuthal scan plot for each interrogation angle.
    a. Move cursor to first X-Y coordinate for first angle.
    b. Draw line from first coordinate to second coordinate.
    c. Continue to draw line from one coordinate to the next

coordinate until 360° azimuthal plane has been covered.

d. Move cursor to first X-Y coordinate for next angle.

e. Repeat steps 4b, c, and d for each interrogation angle.

5. Print interrogation angles next to their respective plots.

Upon completion of the plot, the polar scan routine is executed.

D. A Program to Perform a Polar Scan on a Flaw Along the Vertical Saggital Plane

The polar scan routine utilizes the information gained from the polar plots of the azimuthal scans. As explained, the azimuthal orientation of the flaw determines the VSP for the flaw, based on an ellipsoidal model. The scan routine rotates the multiviewing system about its central axis through an angle that brings transducers 3 and 6 coincident with this azimuthal orientation. A scan in the VSP is then performed from $-\beta_{max}$ to $+\beta_{max}$ in 31 steps. Transducer 3 interrogates the flaw from polar angles $-\beta_{max}$ to 0° and transducer 6 interrogates the flaw from angles $+\beta_{max}/15$ to β_{max}. For each of the polar angles, the radial, axial, and angular positions for the transducer are computed and the transducer moved to those positions. Backscatter data are then taken at that angle. The p-p amplitude is stored for each polar angle. Once the scan is complete, the array of information is written into a file in memory, and an X-Y plotting

routine is executed. The plot of this information is used to determine the polar orientation of the flaw. The algorithm description for the polar scan routine is:

1. Enter azimuthal orientation of the flaw.
2. Read in data file on sample and flaw.
3. Rotate central axis of system. Position transducers 3 and 6 coincident with VSP.
4. Set polar angle to $-\beta_{max}$.
5. Set T/R switch to transducer 6.
6. Compute radial, axial and angular positions for the transducer to interrogate the flaw.
7. Move transducer to positions computed in 6.
8. Acquire backscattering data.
   a. Digitize waveform.
   b. Find p-p amplitude of waveform.
   c. Store p-p amplitude and polar angle.
9. Increment polar angle by $\beta_{max}/15$.
10. Repeat steps 6-9 until polar angle $> 0^{o}$.
11. Set T/R switch to transducer 3.
12. Set polar angle to $+\beta_{max}/15$.
13. Compute radial, axial, and angular positions for the transducer to interrogate the flaw.
14. Move transducer 3 to positions computed in 13.
15. Acquire backscattering data.

a. Digitize waveform.

b. Find p-p value of waveform.

c. Store p-p amplitide and polar angle..

16. Increment polar angle be $+\beta_{max}/15$.

17. Repeat steps 13-16 until polar angle $> \beta_{max}$.

18. Write array of p-p amplitude vs polar angle to data file.

19. Execute X-Y plotting routine.

The source code for these programs, written in the Tektronix Basic language, is included in: "Angular scans for the ultrasonic multitransducer system", James A. Crowder, author, November, 1987. This report is filed with the NDE Center, Iowa State University.

VII. RESULTS

In order to demonstrate that the geometry and position equations derived for the multiviewing system are correct, the scan routines were run on several known samples with flaws. Given the ellipsoidal flaw model used, there are four basic types of flaws that could be interrogated. These are the sphere, the oblate spheroid, the prolate spheroid, and the general ellipsoid. The flaw samples used were made by the Center for Nondestructive Evaluation and the size, shape, and orientation are known. The samples and flaws that were used are:

Sample 1. Oblate spheroidal void in titanium at 0° polar orientation.

Sample 2. Oblate spheroidal void in titanium at 30° polar orientation

Sample 3. Sapphire sphere inclusion in lucite.

Sample 4. Ellipsoidal copper inclusion in lucite.

It should be noted that, for several of the tests, only one of the transducers was functional. For that reason, some of the plots show data for only 180° of the azimuthal or polar plane. Even so, the data presented still illustrate the desired information. The routines were not tested on a prolate spheroidal flaw because there was not a sample available that was suitable for testing.

A. The Azimuthal Scan

Figure 19 shows the result of an azimuthal scan on sample 1. Since the flaw has an oblate spheroidal shape and is at normal incidence to the sample surface, the largest backscatter signal should be obtained when the transducer is normal to the surface of the sample, or at a polar angle of 0°. As the polar angle of interrogation is increased, the backscatter amplitude will decrease. Also, since it is at normal incidence, the peak-to-peak amplitude vs azimuthal angle for a given polar angle should remain constant around the azimuthal plane.

As can be seen from Figure 19, as the azimuthal angle changes for a given polar angle, the peak-to-peak amplitude of the backscatter signal does remain fairly constant. Also, as expected, the largest backscatter amplitude results at a polar angle of 0°. As the polar angle of interrogation increases, the backscatter amplitude decreases.

In contrast, Figure 20 is the result of an azimuthal scan on sample 2, the oblate spheroidal void at a polar orientation of 30°. In this case the sample was situated so that the major axis of the flaw aligned with the -X' axis. With this flaw, the amplitude of the backscatter signal went through a maximum as the scan approached an azimuthal angle of 180°. This happened for every polar angle. A peak occurring at 180° indicates two things. One, the flaw is tilted with respect to the Z' axis and, therefore, cannot be a sphere. Two, it indicates that the flaw is tilted along an azimuthal orientation of

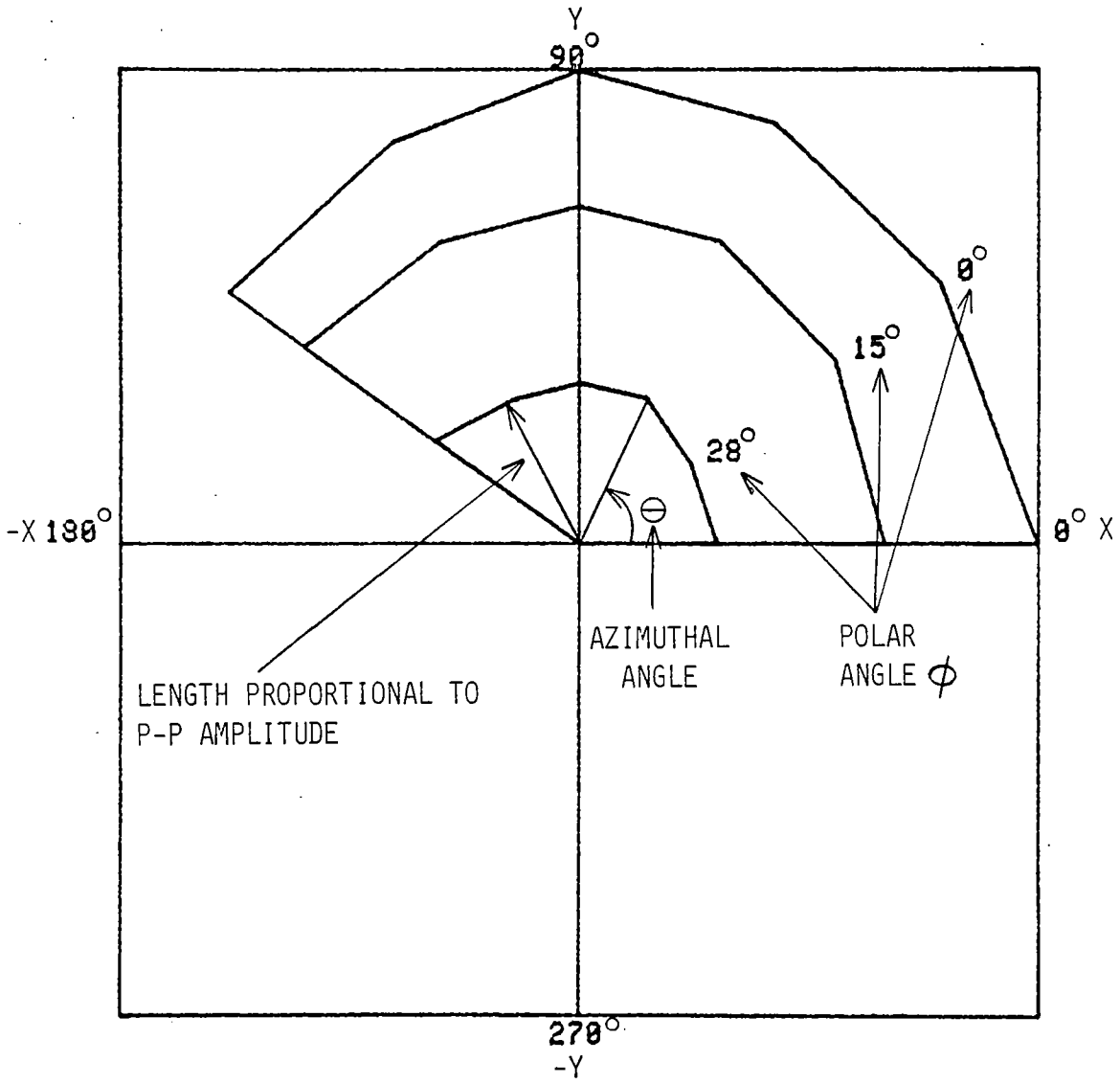

Figure 19. Azimuthal Scan Results of an Oblate Spheroidal Void at Normal Incidence (Sample 1)

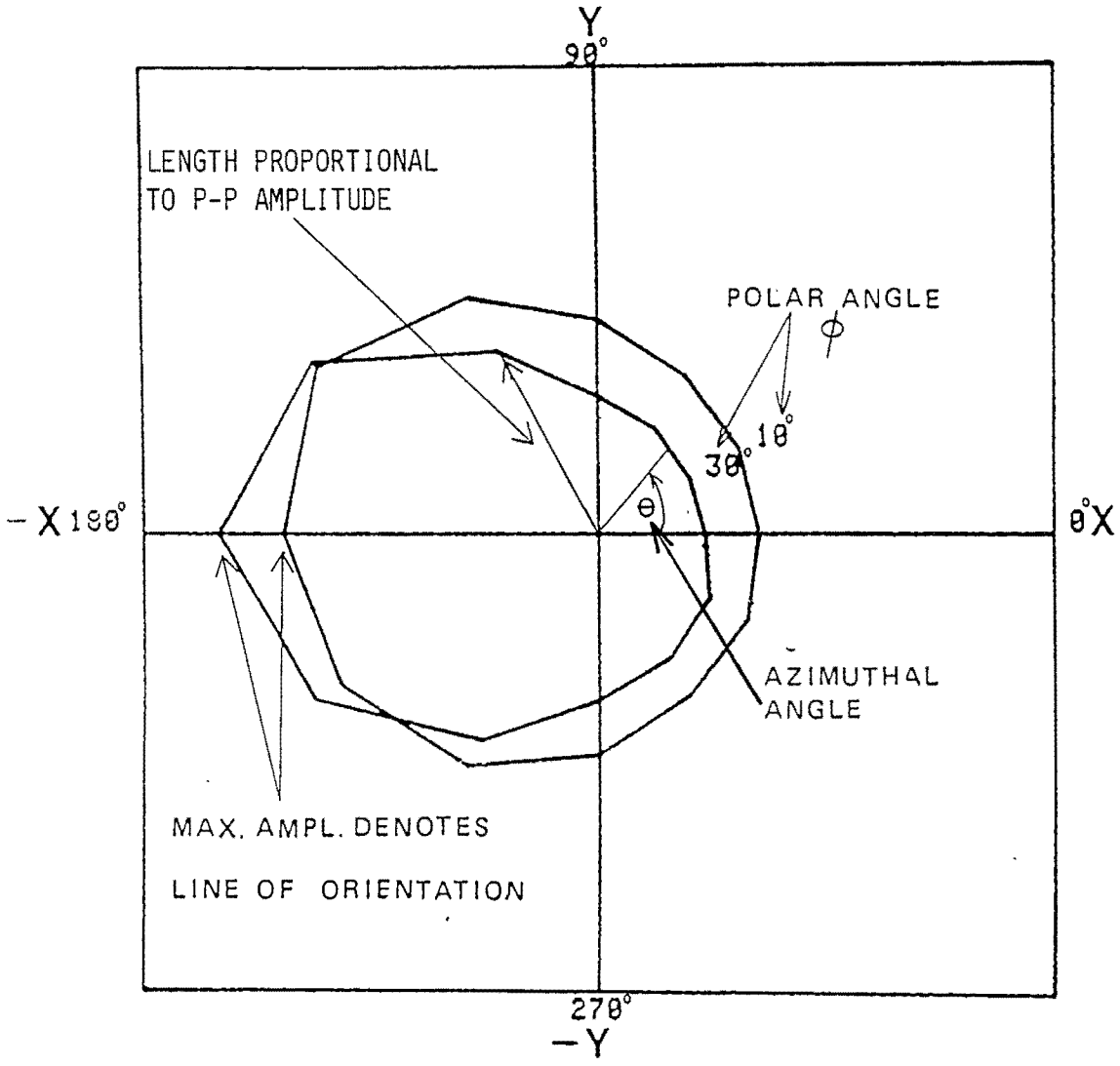

Figure 20. Azimuthal Scan Results of an Oblate Spheroidal Void at a Polar Orientation of 30° (Sample 2)

180^{o}. The plot also indicates that the polar orientation of the flaw must be more than 10^{o} since the plot at an interrogation of 30^{o} has a larger maximum peak-to-peak amplitude than does the plot for a 10^{o} polar angle. The actual determination of this polar orientation is achieved with the polar scan.

The results shown in Figure 21 for sample 3 indicate a radius of curvature and a scattering amplitude that are constant. However, the measured backscatter signal will decrease in amplitude as the polar angle of interrogation is increased because of refraction and attenuation losses. Although attenuation losses are difficult to model [15, 16], they are usually small in comparison to the refraction losses for most materials and can be neglected. The refraction losses are related to the density of the medium, the density of the sample, and the ultrasonic beam angle. There are two refraction losses, one as the beam enters the sample and one as the beam leaves the sample. To account for these losses, a compensation factor was derived based on ultrasonic scattering theory [3, 4, 5, 11]. This compensation factor is given in equation 28, and must be computed for each polar angle of interrogation. The equation for the compenstation factor is:

$$\text{Compensation Factor} = (4*V_w*V_m*\rho_w*\rho_m*\text{Cos}(Wa)/[V_w*\rho_w + V_m*\rho_m*\text{Cos}(wa)]^2) *(4*V_w*\rho_w*V_m*\rho_m*\text{Cos}(Sa)/[V_m*\rho_m + V_w*\rho_w*\text{Cos}(Sa)]^2) \quad (28)$$

where V_w is the velocity of the wave in the water and V_m is the velocity of the wave in the solid. ρ_w is the density of the water, ρ_m is the density of the solid. Wa is the angle of the transducer in the water, and Sa is the angle in the solid.

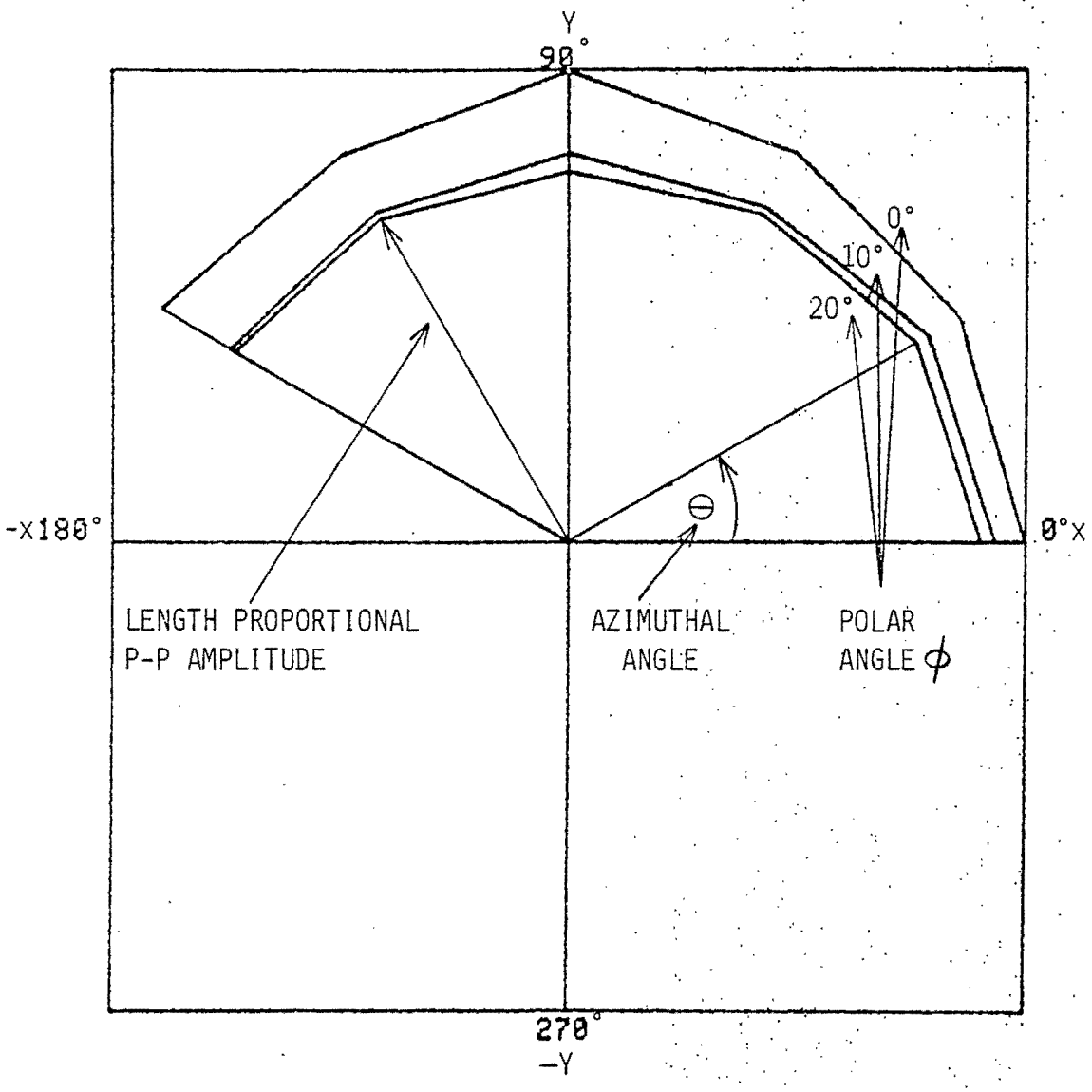

Figure 21. Azimuthal Scan Results of a Sapphire Sphere Inclusion in Lucite (Sample 3)

This loss is present in all of the backscatter signals, but shows up most dramatically with spherical flaws. If there were no attenuation losses, the backscatter signal would be the same from any perspective. In lucite, however, the attenuation factor is appreciable, because ρ_m is much smaller than ρ_w, so there is considerable spacing between the azimuthal plots. Still, there is a marked difference between Figure 21 (sample 3) and Figure 19 (sample 1). Without applying refraction loss compensation, it would be difficult to distinguish between the oblate spheroid at normal incidence and the sphere.

Sample 4 was an ellipsoidal copper inclusion imbedded in lucite and having all three semi-axes of different size. Figure 22 is the plot of an azimuthal scan results. These plots indicate an azimuthal orientation of approximately 135°. As a check to see if the orientation indication was indeed a function of the actual azimuthal orientation, the flaw was rotated 180° about the Z' axis. If the plot in Figure 22 accurately represents the azimuthal orientation of the flaw, the azimuthal scan of the rotated sample should indicate an orientation of 315° or -45°. Figure 23 shows the results of the azimuthal scan performed on the sample rotated 180°. As can be seen, the peak-to-peak backscatter amplitude does indeed go through a maximum at approximately -45° for both of the polar angles of interrogation. This verifies that the original orientation of the flaw is approximately 135°.

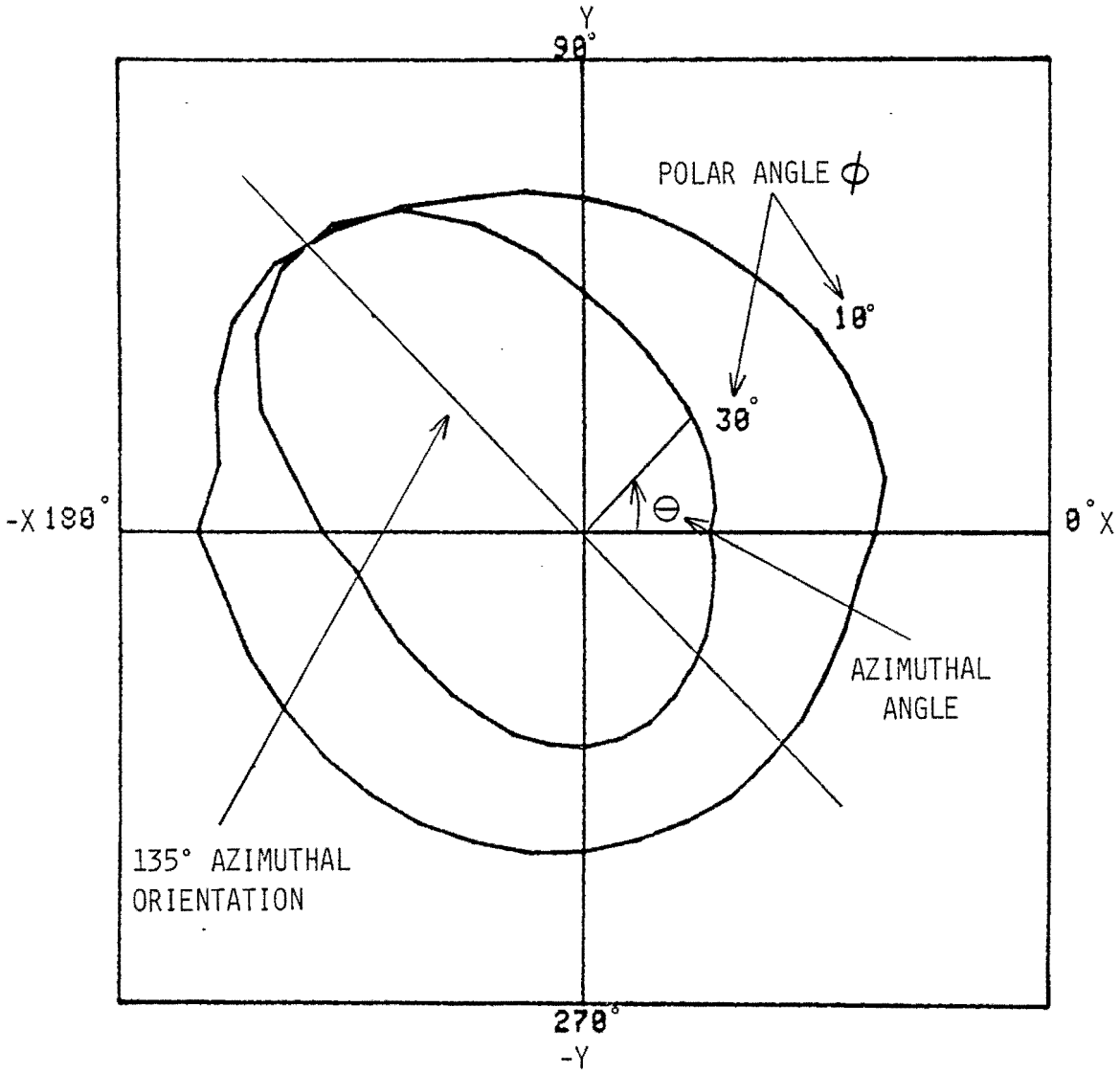

Figure 22. Azimuthal Scan Results of an Ellipsoidal Copper Inclusion in Lucite

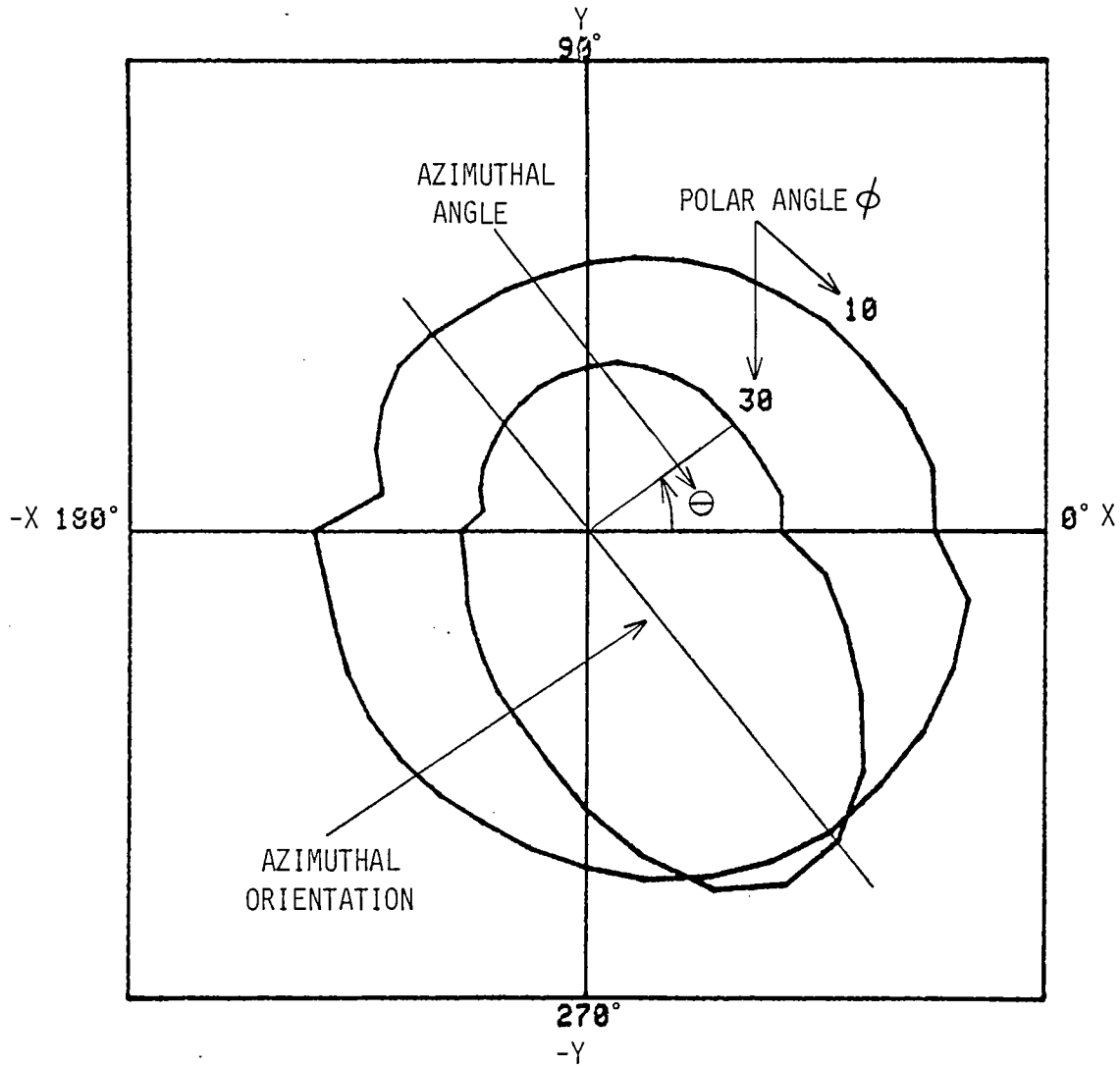

Figure 23. Azimuthal Scan Results of an Ellipsoidal Copper Inclusion in Lucite with 180° Azimuthal Rotation (Sample 4 Rotated About the Z′ Axis)

B. The Polar Scan

As explained earlier, once the azimuthal orientation of the flaw has been determined, a polar scan is performed to determine the polar orientation of the flaw. If no azimuthal orientation is apparent in the azimuthal scan, as is the case for a sphere or an oblate spheroid at normal incidence, the polar scan can provide no further information. However, a detectable azimuthal orientation indicates that the flaw is tilted with respect to the Z' axis and a polar scan should reveal this polar tilt. Figure 24 is an X-Y plot showing the results of a polar scan performed on sample 2. These plots indicate that the maximum p-p amplitude, and therefore the polar orientation of the flaw, is approximately 30^{o}.

Figure 25 is a plot of the polar scan results on sample 4. The amplitude peak indicates a polar orientation of approximately -24^{o}. There are no polar scan results presented for samples 1 and 3. Both of these samples are have flaws with a polar orientation of 0^{o}, and thus a polar scan would not provide additional information.

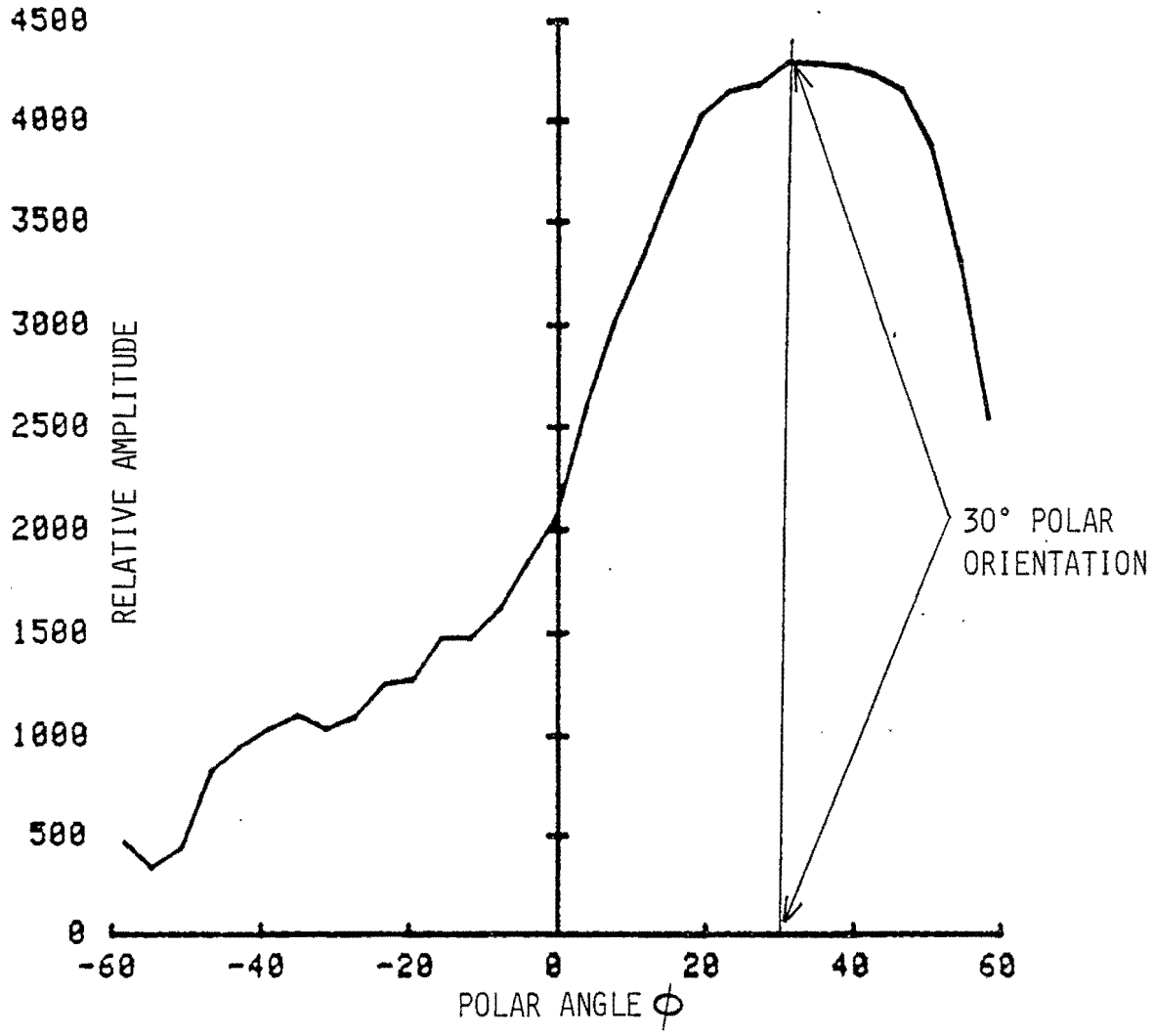

Figure 24. Polar Scan Results of an Oblate Spheroidal Void at 30° Polar Tilt (Sample 2)

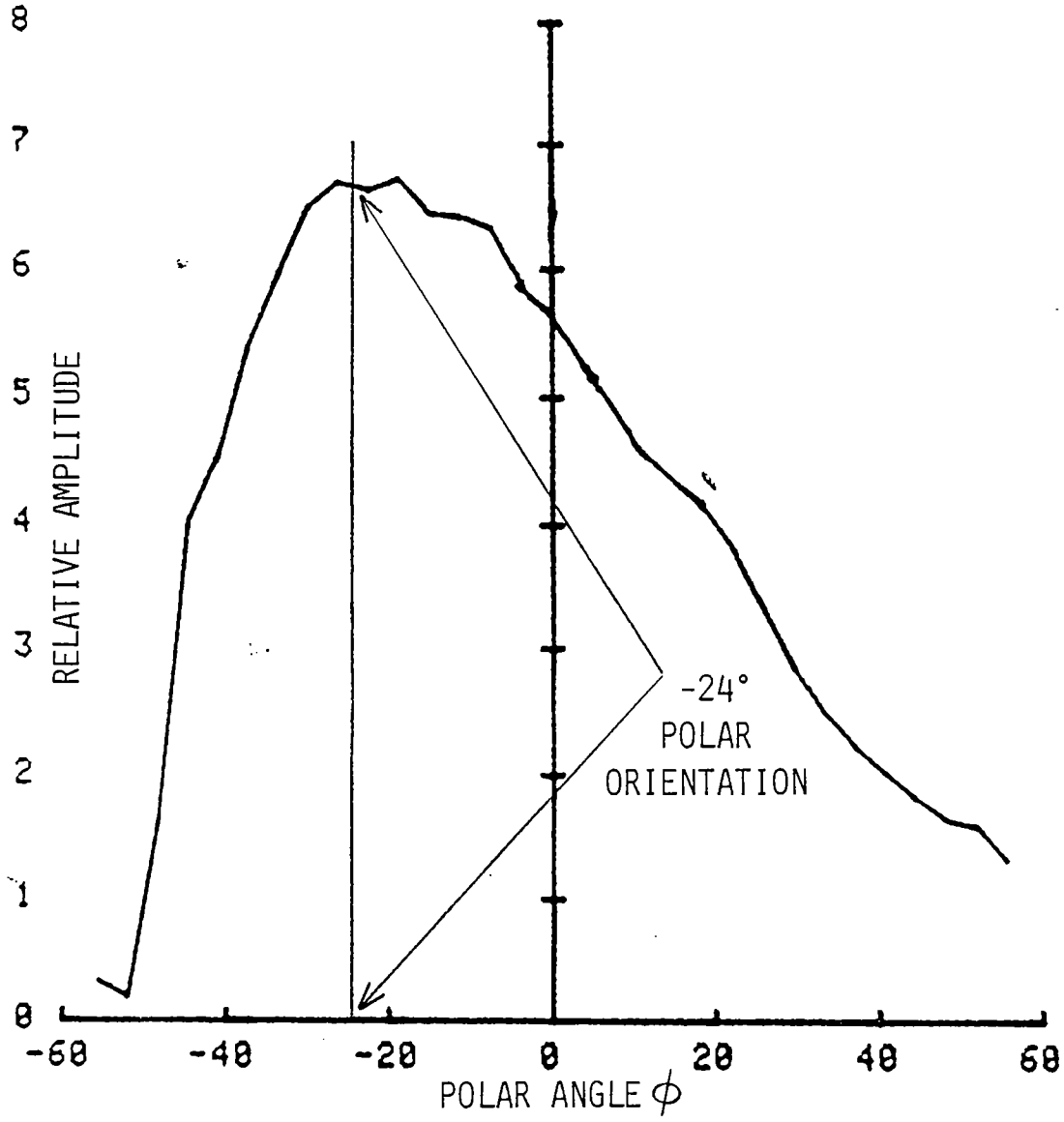

Figure 25. Polar Scan Results of an Ellipsoidal Copper Inclusion in Lucite (Sample 4)

VIII. CONCLUSIONS

The automated azimuthal and polar scan routines developed provide information about the approximate orientation of an ellipsoidal flaw. Such information can be attained in a relatively short period of time, usually ten to twenty minutes. The information attained from these scans is used to design a data acquisition pattern to be used with the flaw reconstruction routines. The acquisition pattern created will provide backscatter data with the largest SNR possible for a given material and flaw.

The flaws tested were not general cases. The test samples were flaws that had only azimuthally and polar rotations. In the general case, the flaw may also have a rotation about the X axis. This is a case that has not been solved yet [9], and creates difficulty in interpreting the scan data. Further investigation is needed to account for this general case if the multiviewing system is to have geveral utility

For future work, the equations and geometry derived for the PSP scan will be used to improve the estivates flaw shape. Also, the equations derived for transducer positions can be used in other scanning processes, such as acoustic microscopy.

IX. ACKNOWLEDGEMENTS

I would like to thank the Center for Nondestructive Evaluation for help during my research work. In particular I would like to thank Sam Wormley and Dr. David Hsu for their guidance and patience in helping me to learn ultrasonics. My thanks and appreciation goes to Dr. Don Thompson for allowing me to do my research work at the center and for introducing me to the fascinating world of nondestructive evaluation. I would also like to thank Dr. Steve Russell for his guidance of my graduate studies.

Most of all, I would like to thank my wife, Karen, for her unending devotion and patience during my graduate work, and for understanding the long nights of studying. I could not have completed my degree without her support and hard work. I would also like to thank her for understanding what drives me to want to do graduate work.

This research work was under the support of the Ames Laboratory Center for Nondestructive Evaluation. Ames Laboratory is operated for the U.S. Department of Energy by Iowa State University under Contract No. W-7405-ENG-82. This work was supported by the Director of Energy Research, Office of Basic Energy Sciences.

X. APPENDIX A:

1-D INVERSE BORN APPROXIMATION

One major step in the flaw reconstruction process is obtaining a size (radius) estimate, r_e, for the flaw in the direction of interrogation. This sizing parameter is calculated from the inversion of the backscatter amplitude [4]. At the Center for Nondestructive Evaluation, the 1-D inverse Born approximation technique has been utilized for such sizing estimates [5, 13, 16, 17, 18]. The overriding equation for the 1-D inverse Born approximation is:

$$\gamma(r) = \text{Constant} * \int_0^\infty A(k)[\text{Sin}(Kr)/(Kr)]dk \qquad (29)$$

where k is the wavenumber, A(k) is the real part of the backscatter amplitude, r is the radius of the flaw, and K is the difference between the absolute magnitudes of the incident and scattering wavevectors (k_i and k_s); i.e. $|K| = |k_i| - |k_s|$ [7].

The function $\gamma(r)$ is a characteristic function from which the flaw size (radius) can be estimated. Theoretically, $\gamma(r) = 1$ inside the flaw and $\gamma(r) = 0$ outside the flaw [7]. The value of r_e, the radius estimate, is the distance from the flaw centroid to the wavefront tangent. This is defined as the value of r such that $\gamma(r) = 1/2$. The radius estimate r_e is shown in Figure 26. As can be seen, this estimate is not an estimate of the radius of the flaw itself.

What is needed is an estimate of the radius r in Figure 26, which is the distance from the flaw's centroid to the boundary tangent. The relationship between r_e and r depends on the flaw's geometry, to be determined.

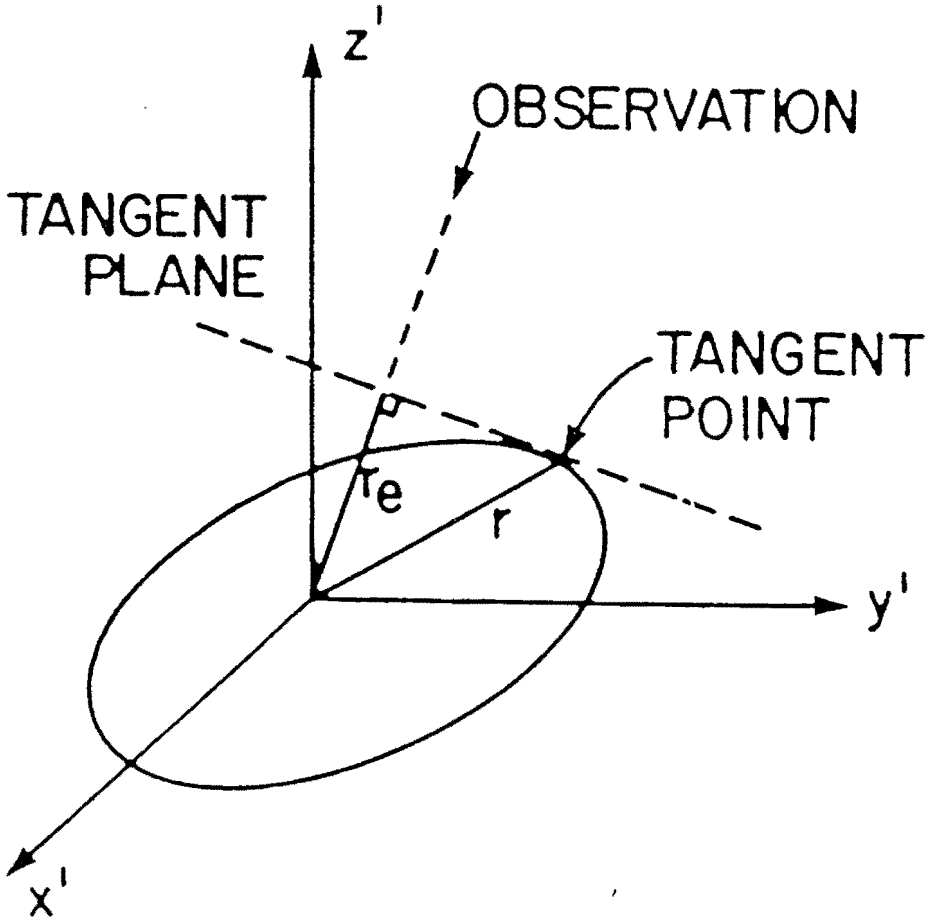

Figure 26. Inverse Born Radius Estimate

In the reconstruction process, it is assumed that the least squares radius estimates obtained from the inverse Born approximation will characterized an ellipsoid. This ellipsoid is described by its three principal axes (a_x, a_y, a_z) and three Euler angles (ϕ, θ, ψ). These angles describe the orientation of the flaw relative to the laboratory coordinate system. To obtain the semi-axes estimates, information from the Born approximation is sent to a nonlinear regression routine. The information takes the form of α', β', and r_e [7], where α' and β' are the azimuthal and polar angles of interrogation respectively, and r_e is from the inverse Born approximation. The tangent plane distance can be expressed in terms of the ellipsoidal semi-axes if it is assumed that the semi-axes system, $\underline{X}$, can be expressed as a transformation, $\underline{B}$, of the laboratory coordinate system, $\underline{X}'$, in the form: $\underline{X} = \underline{B}\underline{X}'$. In this manner, the ellipsoid axes may be represented as:

$$r_e = (a_x^2 I^2 + a_y^2 J^2 + a_z^2 K^2) \tag{30}$$

where I, J, and K are unit vectors computed by:

$$I = b_{11}\mathrm{Sin}\alpha'\mathrm{Cos}\beta' + b_{12}\mathrm{Sin}\alpha'\mathrm{Sin}\beta' + b_{13}\mathrm{Cos}\beta' \tag{31}$$

$$J = b_{21}\mathrm{Sin}\alpha'\mathrm{Cos}\beta' + b_{22}\mathrm{Sin}\alpha'\mathrm{Sin}\beta' + b_{23}\mathrm{Cos}\beta' \tag{32}$$

$$K = b_{31}\mathrm{Sin}\alpha'\mathrm{Cos}\beta' + b_{32}\mathrm{Sin}\alpha'\mathrm{Sin}\beta' + b_{33}\mathrm{Cos}\beta' \tag{33}$$

The b_{ij}s are elements of the transformation matrix $\underline{B}$. The elements of $\underline{B}$ are functions of the three Euler angles ϕ, θ, and ψ. From the thirteen r_e estimates, the equations below are solved iteratively for a_x, a_y, a_z, ϕ, θ, and ψ to find the ellipsoid that best fits the backscatter data, using a least squares approach.

$$x_o' = (1/r_e)[b_{11}a_x^2 I + b_{21}a_y^2 J + b_{31}a_z^2 K] \tag{34}$$

$$y_o' = (1/r\ )[b_{12}a_x^2 I + b_{22}a_y^2 J + b_{32}a_z^2 K] \tag{35}$$

$$z_o' = (1/r\ )[b_{13}a_x^2 I + b_{23}a_y^2 J + b_{33}a_z^2 K] \tag{36}$$

and

$$r = (1/r_e)[a_x^4 I^2 + a_y^4 J^2 + a_z^4 K^2]^{1/2} \tag{37}$$

Utilization of the procedures and equations given here will yield an ellipsoid model of the flaw that best fits the backscatter data acquired. The backscatter data acquired are a series of convolutions involving the driving signal, the impulse response of the scatterer, and the transducer response function modified by diffraction and attenuation effects [15, 19]. The Fourier transform of the equation describing the recieved backscatter signal is:

$$M(\omega) = \beta(\omega)T(\omega,z)S(\omega,a,\theta) \tag{38}$$

where $M(\omega)$ is the recieved backscatter signal, $\beta(\omega)$ describes the transducers response to an excitation voltage, $T(\omega,z)$ describes the diffraction and attenuation losses as well as other

propogation characteristics, and $S(\omega,a,\theta)$ is the absolute scattering amplitude function of the flaw.

Through a deconvolution process, the absolute scattering amplitude is extracted [14, 15] and used in the inverse Born approximation. The function $T(\omega,z)$ provides the diffraction and attenuation corrections as a function of frequency.

XI. APPENDIX B:

THE MULTIVIEWING ULTRASONIC TRANSDUCER SYSTEM

A. Overall Description

The automated multiviewing ultrasonic system, called a disparity detector, was designed by Ames Laboratory for the purpose of ultrasonic flaw investigation. It was designed to provide the flexibility of interrogating a flaw within a solid material from any perspective desired, and to have the ability to view the flaw from many perspectives at the same time with little or no mechanical motion. The original intent of the design was to reconstruct flaws using inverse scattering theories. However many other uses for the device may be investigated such as ultrasonic microscopy.

Figure 27 shows an photograph of the overall system as it resides in its water tank. Figure 28 is a photograph of an individual transducer showing the degrees of freedom for each transducer. Each transducer may be moved radially toward the central axis of the system, tilted toward the central axis, and may be moved along its own acoustic axis. This last movement is used to accomplish acoustic wave propogation time equalization. The entire disparity detector may be moved in the X′-Y′-Z′ laboratory coordinate space, and it may be rotated about its central axis. The X′-Y′ freedom allows the

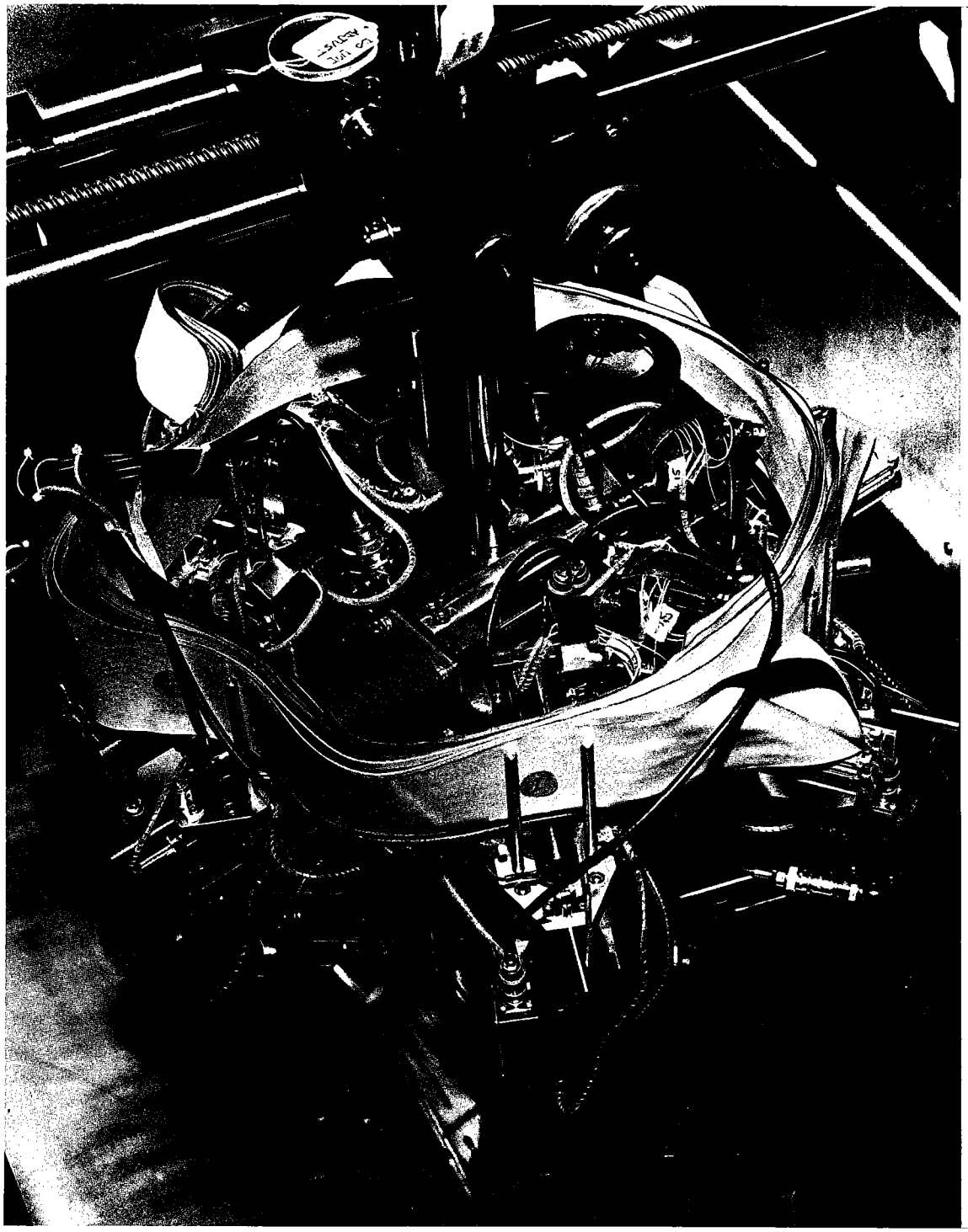

Figure 27. Multiviewing Ultrasonic Transducer System

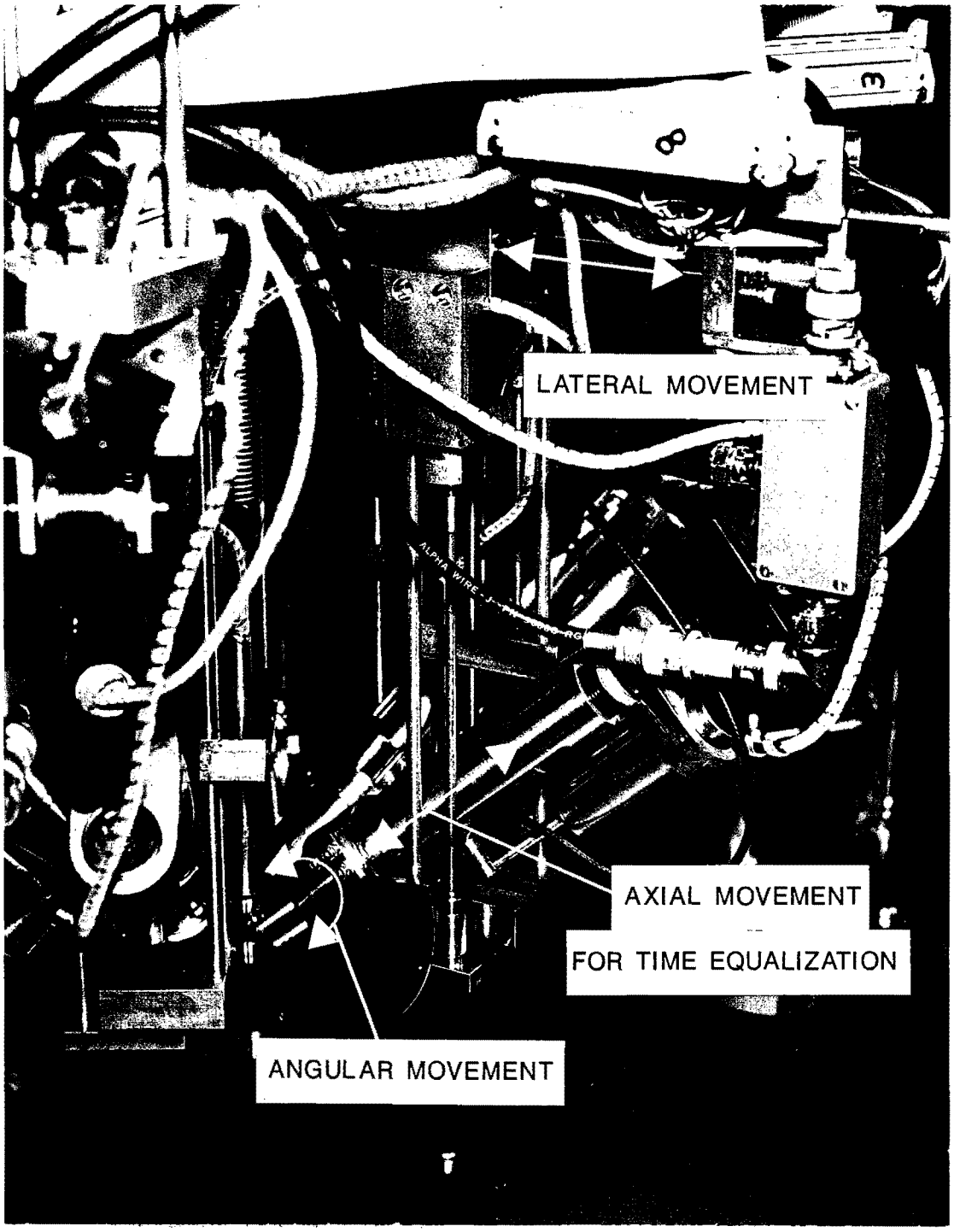

Figure 28. Degrees of Freedom for Individual Transducer

disparity detector to be positioned over a flaw for interrogation. Figure 29 shows the six transducers focused on a flaw for multiple interrogation. The Z' freedom allows for setting of the initial acoustic wave propogation time. The rotation about the central axis gives the disparity detector the ability to position a transducer at any azimuthal angle.

B. Transducer Positioning Convention and Limits

The definitions of the radial movements for the transducers are shown in Figure 30. This is a view looking down the Z' axis onto the transducers. Two of the transducers, number 3 and number 6, may be moved radially inward until coincident with the central axis. The other four transducers may be moved approximately one-half the distance from the outer limit to the central axis. The convention for the absolute positioning distances in given in Figure 30. The circle denoting the center of travel for each transducer is marked as 0 cm. From this point the central axis is 5.698 cm. radially inward. This is considered a negative movement and is shown as -5.698 cm. The outside limit of movement is 5.7325 cm. from the center. Since the movement from the center to this position is radially outward, it is considered to be the +5.7325 cm. position, and the limits of motion for transducers 3 and 6 are +5.7325 cm. to -5.698 cm. The limits for the other four transducers are +5.7325 cm. to -0.3 cm.

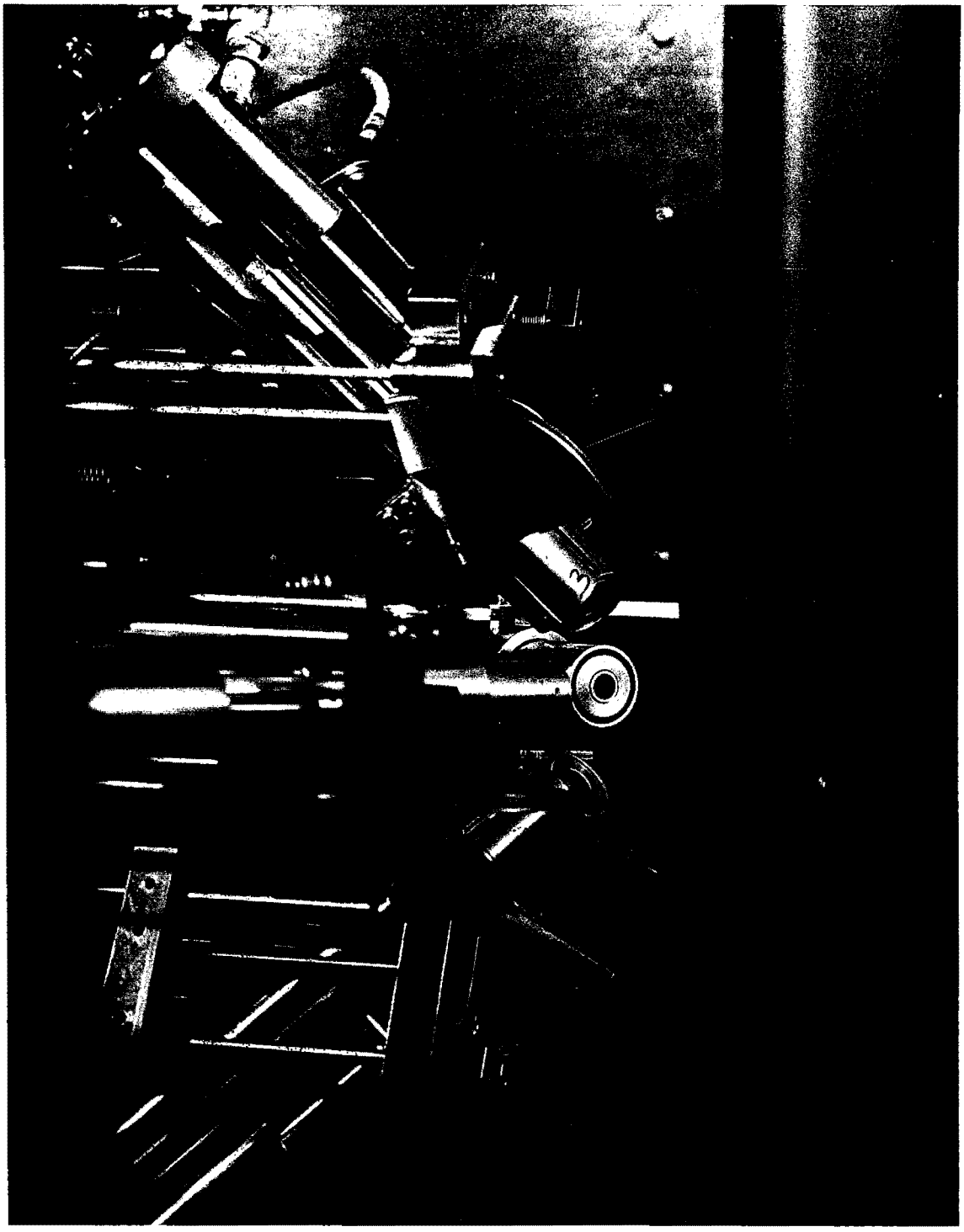

Figure 29. Multiple Interrogation

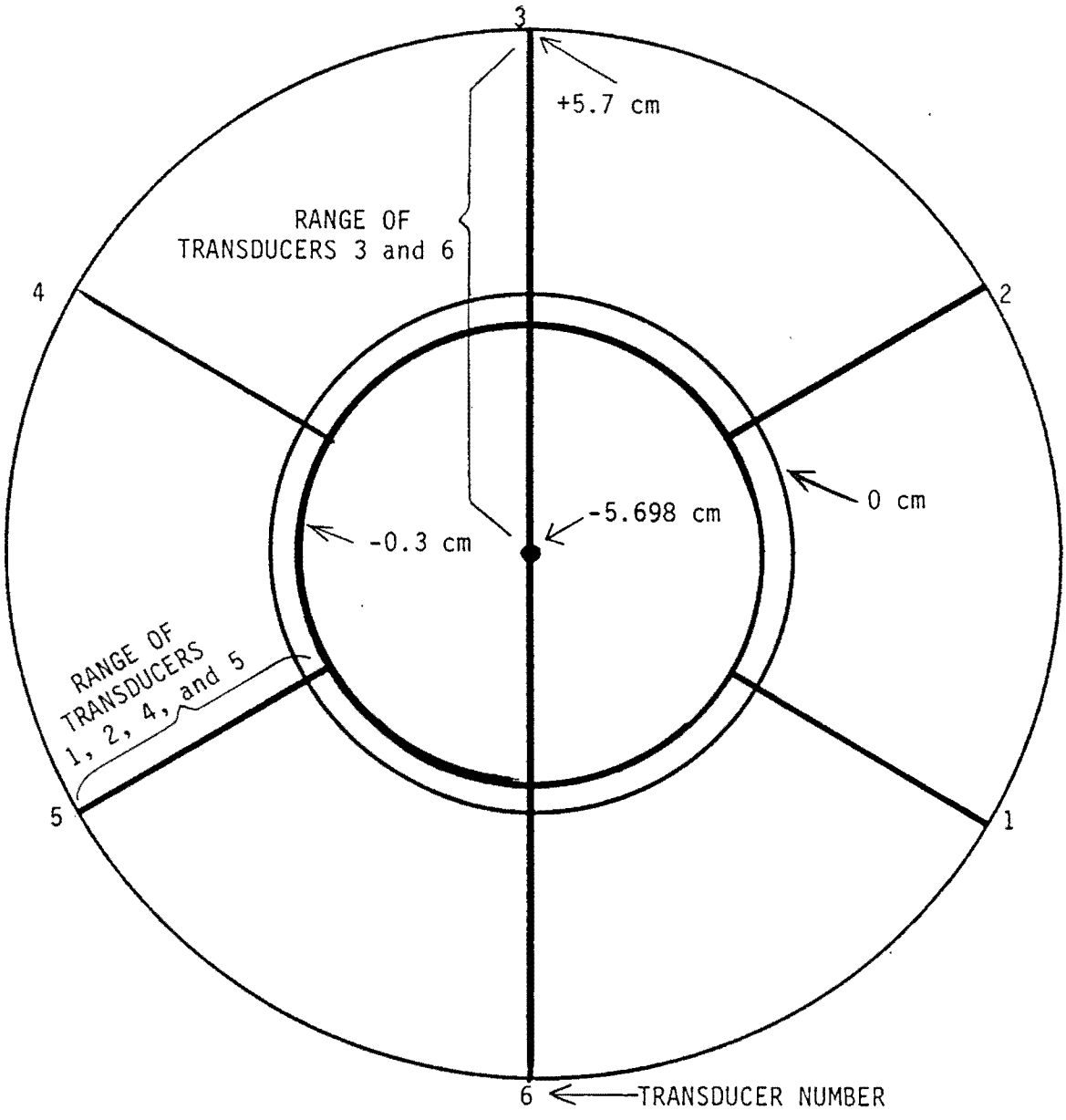

Figure 30. Radial Motion Definitions

For the angular movement, the absolute transducer position are referenced from the 0^{o} or upright position. It is considered a positive movement when the transducer is tilted toward the central axis and a negative movement when the transducer is tilted away from the central axis. The limits of tilt for each transducer are from $+60^{o}$ to -5^{o}. The axial positions from the transducers are referenced relative to the transducer housing. The convention is such that the 0 cm. position for any transducer is when the transducer is flush with the transducer housing. Moving the transducer out from the transducer housing is considered a positive movement. The limits of the axial motion are 0 cm. to +5 cm.

C. Electronics

The motors that are used to position the transducers are controlled by a 6809 processor. Each of the 18 transducer motors and the central axis rotation motor is a digitally driven stepper motor. The 6809 processor is connected to the Tektronix 4052 host computer through a GPIB interface.

D. Ultrasonic Signal Flow

Figure 31 is a block diagram of the ultrasonic signal flow for the multiviewing system.

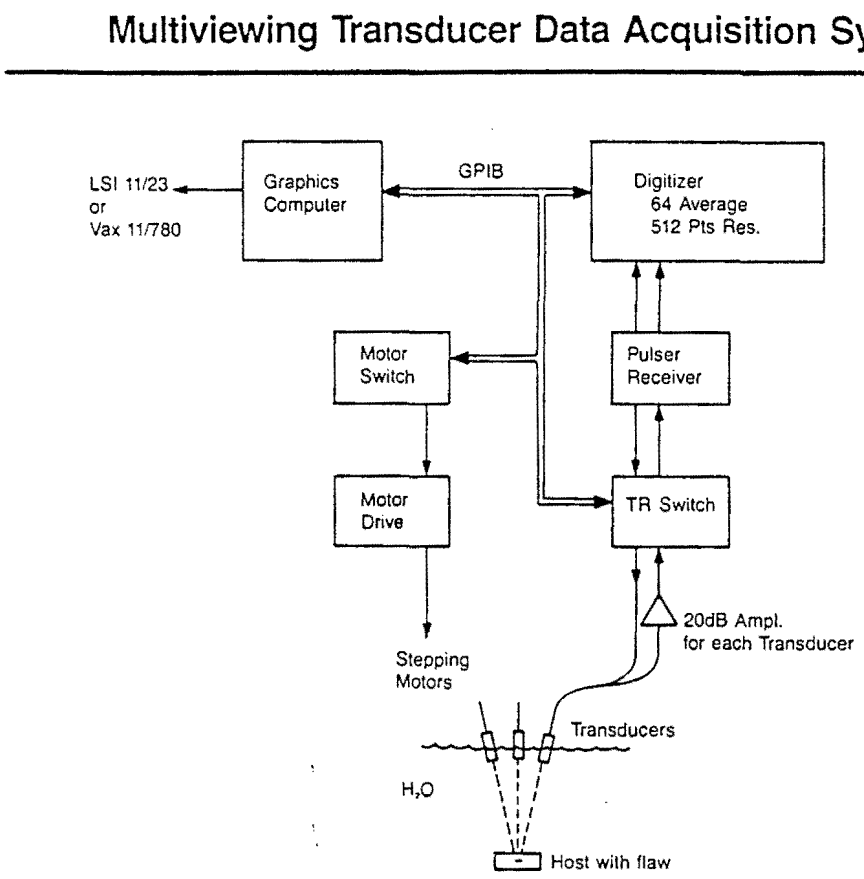

Figure 31. Ultrasonic Signal Flow

XII. BIBLIOGRAPHY

1. S. J. Wormley and D. O. Thompson, "Error sensibility of long and intermediate wavelength flaw reconstruction". Review of Progress in Quantitative NDE, Vol. 4A. Edited by D. O. Thompson and D. E. Chimenti (Plenum Press, New York, 1985), 203-211.

2. D. O. Thompson and S. J. Wormley, "Absolute magnitude of front surface reflections in ultrasonic measurements". Review of Progress in Quantitative NDE, Vol. 3A. Edited by D. O. Thompson and D. E. Chimenti (Plenum Press, New York, 1984), 382-393.

3. J. D. Achenback, A. D. Gautesen, and H. McMaken, Ray Methods for Waves in Elastic Solids (Pitman, New York, 1982), 345-390.

4. J. H. Rose, R. K. Elsley, B. R. Tittmann, V. V. Varadam, and V. K. Varadam, "Inversion of ultrasonic scattering data", Acoustic, Electromagnetic, and Elastic Wave Scattering--Focus on the T-matrix Approach (Pergamon Press, New York, 1980), 605.

5. J. H. Rose and J. A. Krumhansl, "Determination of flaw characteristics from ultrasonic scattering data", J. Appl. Phys. 50, 2951 (1979).

6. J. M. Richardson and K. Fertig, in Proc. DARPA/AF Review of Progress in Quantitative NDE, AFWAL-TR-80-4078, 528 (1978).

7. S. J. Wormely, D. K. Hsu, and D. O Thompson, "The effects of flaw orientation and finite aperture on model-based reconstruction using multiprobe transducers". Review of Progress in Quantitative NDE, Vol. 5A. Edited by D. O. Thompson and D. E. Chimenti (Plenum Press, New York, 1986), 585-594.

8. S. J. Wormely, J. A. Crowder, and D. O. Thompson, "An automated multiviewing ultrasonic system for reconstruction of arbitrarily oriented flaws". Review of Progress in Quantitative NDE, Vol. 8A. Editied by D. O. Thompson and D. E. Chimenti (Plenum Press, New York, 1988) to be published.

9. D. O. Thompson, S. J. Wormley, and D. K. Hsu, "An apparatus and technique for reconstruction of flaws using model-based elastic wave inverse ultrasonic scattering", Rev. Sci. Inst., 57(12), 3089-3098 (1986).

10. B. P. Newberry, J. A. Gray, E. F. Lopes, and R. B. Thompson, "Evaluation of ultrasonic beam models for the case of piston transducers radiating through a liquid-solid interface". Review of Progress in Quantitative NDE, Vol. 5A. Edited by D. O. Thompson and D. E. Chimenti (Plenum Press, New York, 1986), 127-138.

11. D. K. Hsu, S. J. Wormley, and D. O. Thompson, "Characterization of flaw shape and orientation using ultrasonic angular scans". Review of Progress in Quantitative NDE, Vol. 6A. Edited by D. O. Thompson and D. E. Chimenti (Plenum Press, New York, 1987), 585-594.

12. D. O. Thompson and S. J. Wormley, "Long and intermediate wavelength flaw reconstruction". Review of Progress in Quantitative NDE, Vol. 4A. Edited by D. O. Thompson and D. E. Chimenti (Plenum Press, New York, 1985), 287-296.

13. E. Domany, K. E. Newman, and S. Teitel, "Elastic wave scattering by general shaped defects", Proc. DARPA/AF Review of Progress in Quantitative NDE, AFWAL-TR-80-4078, 341 (1978).

14. D. Elsley, J. M. Richardson, and R. Addison, "Optical measurements of broadband ultrasonic data", Ultrasonic Symposium Proceedings, 2, 916-921 (1980).

15. R. B. Thompson and T. A. Gray, "A model relating ultrasonic measurement through liquid-solid interfaces to unbound medium scattering amplitudes", J. Acoust. Soc. Am. 74(4), 1279-1288 (1983).

16. D. K. Hsu, J. H. Rose, and D. O. Thompson, "Reconstruction of inclusions in solids using ultrasonic Born inversion", J. Appl. Phys., 55(1), 162 (1984).

17. J. H. Rose and J. L. Opsal, "Inversion of ultrasonic scattering data". Review of Progress in Quantitative NDE, Vol. 1. Edited by D. O. Thompson and D. E. Chimenti (Plenum Press, New York, 1982), 573.

18. V. G. Kogan and J. H. Rose, "On the effects of a finite aperture on the inverse Born approximation". Review of Progress in Quantitative NDE, Vol. 2A. Edited by D. O. Thompson and D. E. Chimenti (Plenum Press, New York, 1983), 1141.

19. B. R. Tittmann, D. O. Thompson, and R. B. Thompson, "Standards for quantitative examination", Nondestructive Testing Standards. Edited by Harold Berger (ASTM, Philadelphia, 1976), 295.